# PRODUCTION OF LUTETIUM-177 VIA THE INDIRECT ROUTE USING PUR-1

by

**True Miller**

**A Thesis**

*Submitted to the Faculty of Purdue University*

*In Partial Fulfillment of the Requirements for the degree of*

**Master of Science in Nuclear Engineering**


School of Nuclear Engineering

West Lafayette, Indiana

May 2021

**THE PURDUE UNIVERSITY GRADUATE SCHOOL**
**STATEMENT OF COMMITTEE APPROVAL**

**Dr. Yunlin Xu Chair**
School of Nuclear Engineering

**Dr. Robert S. Bean**
School of Nuclear Engineering

**Dr. Jason T. Harris**
School of Health Sciences

**Approved by:**
Dr. Seungjin Kim

# TABLE OF CONTENTS

# LIST OF TABLES

# LIST OF FIGURES

# NOMENCLATURE

| | |
|---|---|
| AGOT | Acheson Graphite Ordinary Temperature |
| ARO | All Rods Out |
| BFCA | Bifunctional Chelating Agent |
| CF | Carrier Free |
| CFD | Computational Fluid Dynamic |
| CORO | Committee on Reactor Operations |
| CRH | Critical Rod Height |
| CP1 | Chicago Pile 1 |
| EOB | End of Burnup |
| HDPE | High Density Polyethylene |
| HEU | High Enriched Fuel |
| HFIR | High Flux Isotope Reactor |
| HPGe | High Purity Germanium |
| LEU | Low Enriched Fuel |
| MC | Monte Carlo |
| MCNP | Monte Carlo Neutral Particle |
| NCA | No-Carrier-Added |
| NRC | Nuclear Regulatory Commission |
| ORIGEN | Oak Ridge Isotope Generation Code |
| PCM | Percent Mille |
| PET | Positron Emission Tomography |
| PuBe | Plutonium Beryllium |
| RIT | Radioimmunotherapy |
| TRT | Targeted Radionuclide Therapy |

# ABSTRACT

The use of high flux research reactors, such as the High Flux Isotope Reactor (HFIR), to produce a wide variety of both industrial and medical isotopes has been well documented and proven to be economically feasible. However, due to the lack of access to these high flux facilities by most countries, isotope production methods utilizing reactors with low to moderate flux levels are needed, especially for short lived medical isotopes whose production must be relatively close to the location where they will be administered. In recent years medical isotopes that can both be used for treatment and diagnostic uses have become of great interest. One of the most popular of these theragnostic radionuclides is lutetium-177. Production of high-grade Lu-177 can be achieved in both high and low flux reactors through two different production methods. The current work looks to determine the feasibility of producing Lu-177 via the indirect route, using the relatively low flux of PUR-1. This will be accomplished through the use of high-fidelity models and simulations to predict the resulting production rates of the desired products. The results of these models and simulations will then be compared to the results obtained from the experimental irradiation of various samples of ytterbium oxide in PUR-1. Many studies have successfully produced Lu-177 using moderate and high flux reactors and several papers have studied the predicted production rate for low to moderate flux reactors by using the reported thermal flux of various research reactors and the reported cross-section values for ytterbium. A Monte Carlo based model of PUR-1 will be developed to determine the radiative capture reaction rates for the ytterbium targets across all neutron energies. This model in conjunction with a simplified MATLAB model, to solve the series of partial differential equations describing the production and decay of each product isotope, will be used to predict isotope production rates and will be compared to experimentally obtained results.

# 1. INTRODUCTION

## 1.1 Project Overview

This project is a joint collaboration between the Purdue School of Nuclear Engineering and Niowave, Inc. Niowave is a company located in Lansing, Michigan that specializes in the production and supply of medical and industrial isotopes. This project is meant to test the feasibility of using PUR-1 to produce the medical radionuclide Lutetium-177. PUR-1 is a low power pool-based research reactor, located at Purdue University, with a maximum power of 10 kW. Due to this relatively lower power allowed, the reactor is only capable of producing a thermal flux on the order of magnitude of $4 \times 10^{11}$ n/cm$^2$-s whereas full power research reactors are capable of reaching fluxes of $1 \times 10^{14}$ to $1 \times 10^{15}$ n/cm$^2$-s. Through this collaboration Niowave will provide irradiation capsules and the ytterbium oxide target material for us to irradiate in PUR-1. With this project the maximum amount of Lu-177 that can be produced with PUR-1 is hoped to be determined. This general scoping study will allow Purdue to test PUR-1's new abilities now that it has had a power upgrade to 10 kW and an entirely digital control and data monitoring system installed. At the same time Niowave will receive the Lu-177 that is produced in these studies which will allow for them to test various chemical separation methods for removing the Lu-177 from the ytterbium target material. This study will provide a basis for the feasibility of producing medical and industrial isotopes using the PUR-1 research reactor.

## 1.2 Background

Therapeutic radioisotopes have become an increasingly important tool in the medical field. Many radioisotopes are used today for the treatment of cancers due to their ability to deliver a concentrated dose of radiation to highly targeted parts of the body with negligible dose to the surrounding tissues. Radioisotopes also play an important role in medical imaging techniques such as positron emission tomography (PET) and allow for new diagnostic tools for detecting and diagnosing various illness. Most medical isotopes used today are neutron rich and are typically beta minus emitters. As such these radioisotopes are mostly produced in research reactors by bombarding a stable isotope with neutrons into an activation product which then decays into the

radioisotope of interest. The ideal neutron flux and irradiation time is entirely dependent on the target material as well as the nuclear properties of the isotope being produced.

There are many factors which will affect the overall yield of a radioisotope when using a reactor for production. The maximum theoretical yield of the isotope of interest will be dependent on the flux delivered to the target material, the neutron capture cross-section of the target isotope and the half-life of the desired product. When the rate of production is equal to the rate of decay of the product the material has reached its saturation value. The saturation value is the highest yield theoretically possible, but this value is typically never reached due to several other limiting factors. Other factors that determine the production rate are self-shielding in the target, variation in the reactor power, burnup of the target isotope due to subsequent neutron captures after production, and depletion of the target material over time [1]. In general, the higher the neutron flux the reactor is able to operate at the greater the production rate will be.

### 1.2.1 Medical Isotopes

Medical isotopes are typically produced by placing a target material in a sealed canister or capsule which is then placed in an irradiation port of a reactor. This capsule is then irradiated by the neutron flux for a predetermined period of time at which point the capsule is removed and the irradiated material is processed. There are several properties necessary for a radioisotope to be a good medical isotope candidate. The first requirement is for the target isotope to have a large neutron capture cross-section. If the reaction cross-section is not sufficiently large, even with a very high neutron flux, the production rate will be inadequate. The target material must also be available with high purity to avoid the production of unwanted isotopes from neutron capture by the impurities in the target. For the same reason it is desirable to have a target material that is isotopically pure or enriched to a high degree with the desired target isotope. Ideally the product isotope will also be a different chemical species than what is present in the target material so that chemical processes can be used to separate the two. By being able to separate the product isotope from the target material the activity per unit mass will be very high, typically near the theoretical limit, this value is known as the specific activity and is of great importance when it comes to medical isotopes. If the product isotope is of the same chemical species as the target material this type of separation is impossible and it is impossible to produce what is known as no-carrier-added (NCA) radionuclides and the resulting specific activity of this material may be low [1]. Lastly, for

a radioisotope to be of medical value it must have a desirable type and energy of radiation being emitted in addition to an appropriate half-life. If the half-life is too short, then it is prohibitively difficult to administer the medicine to a patient before a majority of it has decayed away. On the other hand, if the half-life is too long then the radiation dose rate, which is inversely related, will be too low and spread out to be of use.

### 1.2.2 Isotope Production Methods

There are multiple mechanisms that can be used to produce different radioisotopes. These routes are based on the various neutron-particle interactions that exist. The most common production route is through the direct activation of the material by neutron capture and gamma emission. This is known as the radiative route and is most effective with target material that is isotopically and chemically very pure and possesses a very high neutron absorption cross-section. For this direct route of production, the highest level of flux that can be obtained is desirable in order to convert as much of the target material into the desired product as possible before a significant amount of the product has had time to undergo decay. Since the product isotope is of the same chemical species as the target this method typically produces a lower specific activity material than other methods. An example of the radiative route is the production of Samarium-153, with a 1.9-day half-life, which is currently used to treat bone cancer [2].

$$^{152}Sm(n,\gamma) \rightarrow {}^{153}Sm$$

Medical radioisotopes can also be produced through an (n,p) reaction where a neutron knocks a proton free from the nucleus of the target atom. Most (n,p) reactions have a high threshold energy for the reaction, typically above 2 MeV. As a result the fast flux is much more important than the thermal flux, in the neutron spectrum, for production using this method. Since most reactors have a much higher thermal flux than fast flux the ideal target material for this production route should have a very low thermal neutron cross-section to minimize the number of undesirable reactions. Most research reactors do not have a significant fast flux spectrum compared to their thermal flux, this results in a small production rate of the desired isotope and necessitates chemical separation of the product from the target material. Despite the low production rates using this route a no carrier added (NCA) radionuclide product can be produced with this method producing a high

specific activity material. Strontium-89 is produced using this production route, Strontium-89 is used to treat bone metastases from prostate cancer and has a half-life of 50.5 days [3].

$$^{89}Y(n,p) \rightarrow {}^{89}Sr$$

A third production route is through an (n, $\gamma$) reaction followed by a subsequent beta decay to obtain the isotope of interest. This method has several advantageous over the two methods previously discussed. Target materials with high cross-sections for (n, $\gamma$) reactions can take advantage of the large thermal flux present in most research reactors, allowing for high production rates of the precursor isotope which then decays via beta decay into the desired radioisotope. Since the desired isotope is then chemically different from the target material chemical separation of the product from the target can be employed to achieve a very high specific activity material. This method combines the benefit of the high reaction cross-sections from the (n, $\gamma$) route and the benefit of the product being chemically different, similar to the (n,p) method. Ideal candidates for this production method possess a large cross-section for the target isotope but a small neutron cross-section and short half-life for the intermediate isotope as to avoid a second neutron absorption from occurring before the beta decay can happen. Iodine-131, which can be used to treat hyperthyroidism and thyroid cancer, is produced using this production route.

$$^{130}Te(n,\gamma) \rightarrow {}^{131}Te \xrightarrow{\beta^-} {}^{131}I$$

Additional methods for medical isotope production can also include (n,$\alpha$) reaction routes as well as the chemical separation of fission products such as Molybdenum-99 which decays into the medically useful Technetium-99m.

### 1.2.3 Lutetium-177

In recent years interest in radioisotopes with low to medium energy betas and low energy gamma emissions capable of both diagnostic and therapeutic applications has grown significantly. These theragnostic radionuclide allow for real time gamma imaging before and during treatment coupled with soft tissue penetration ranges of only a couple millimeters [1]. One isotope in

particular, Lutetium-177, has grown in interest and importance over the last several years and displays all of these favorable characteristics of a theragnostic radioisotope. The popularity of Lutetium-177 has taken off in the last half-decade or so due to its favorable characteristics for use in targeted radionuclide therapy (TRT). TRT is a type of target molecular therapy where through the use of peptides specifically designed to fit the cell surface receptors, which are overproduced on tumor cells, the radionuclide is then delivered directly to where it is needed [5]. Lu-177 has a 6.64-day half-life and decays into the stable isotope Hf-177. This long half-life allows for a sufficient amount of time to refine and produce medicines from the isotope and allows for production to be located far away from the final end use location. Lu-177 emits medium to low energy betas with maximum energies of 497 keV, 384 keV and 176 keV. The mean penetration range of these betas in soft tissue is 670 $\mu$m making it an ideal radionuclide for delivering its energy to a small volume [5]. Lu-177 also emits low energy gamma rays with energies of 208 keV and 113 keV during its decay. These gammas allow for dosimetry to be performed both before and during the administration of the medicine as well as imaging the biodistribution of the isotope. A simplified decay scheme of Lutetium-177 can be seen below in Figure 1.1.

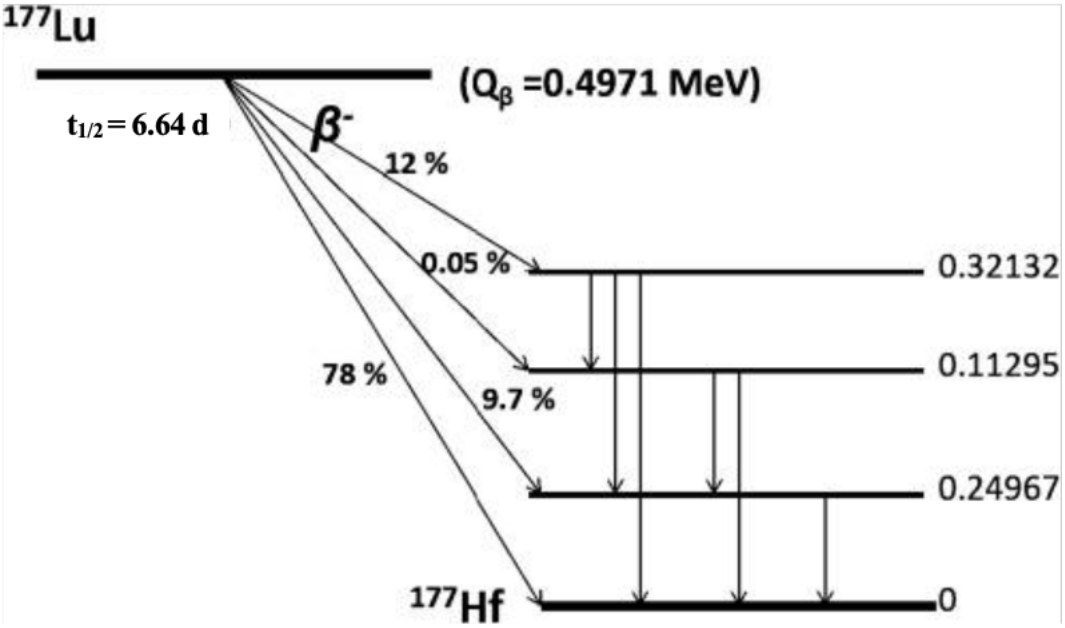


Figure 1.1. Simplified decay scheme of Lu-177 [5].

The use of Lutetium-177 is not only advantageous for TRT due to its favorable half-life and decay characteristics but also due to its unique chemical nature. Lutetium only exists in its +3 oxidation state which rules out any chemical or solubility changes to the medicine that may occur due to oxidation and reduction reactions. Additionally, lutetium forms nine different coordination complexes making it very useful for producing a range of different molecular carriers such as peptides, proteins, antibodies, and small molecules [5]. Lutetium in its +3 state is also suitable for peptide and protein radiolabeling by attaching it to the molecule of interest using what is known as a bifunctional chelating agent (BFCA) [5]. A large variety of Lutetium-177 based pharmaceuticals for a multitude of uses has been developed in recent years. Lu-177 labeled radiopharmaceutical uses currently include peptide receptor radionuclide therapy for treatment of neuroendocrine tumors, for bone palliation of metastatic cancer, for radiation synovectomy and radioimmunotherapy [1].

### 1.2.4 Lutetium-177 Production Methods

There are two main pathways to the production of Lutetium-177, as seen in Figure 1.2, both involving the use of a neutron flux from a reactor and both with their own benefits and drawbacks. Lu-177 can either be produced by what is known as the 'direct route' where Lu-176 is transmutated to Lu-177 via an (n, $\gamma$) reaction, or through the 'indirect route' where Yb-176 is first transmutated into Yb-177 via an (n, $\gamma$) reaction and then it subsequently decays into Lu-177 via beta decay with a 1.91-hour half-life.

$$^{176}Lu(n,\gamma) \rightarrow {}^{177}Lu$$

$$^{176}Yb(n,\gamma) \rightarrow {}^{177}Yb \xrightarrow{\beta^-} {}^{177}Lu$$

Both pathways have been proven to be viable options. Which production route is best is dependent on the flux level of the reactor being used for production as well as what quality of end product is desired.

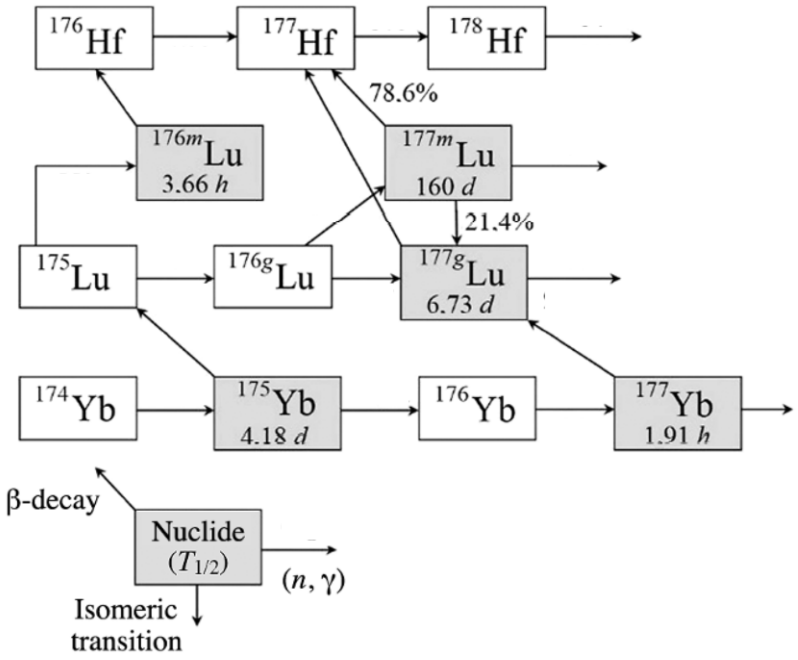


Figure 1.2 Nuclear transmutation pathways for the production of Lu-177 [6].

***Direct Route***

The direct production method is the least complicated way to produce Lu-177 but requires reactors with a relatively high neutron flux. Typically, $Lu_2O_3$ will be used as the target material with either natural lutetium or one that has been enriched to increase the percentage of Lu-176 in the target. Enriched targets are often used as the natural abundance of Lu-176 is very low at approximately only 2.6%. With a large enough thermal flux however, Lu-175 may undergo two neutron captures to eventually produce Lu-177 as well. In most circumstances though this production pathway is negligible. With enriched material a large percentage of the target can be converted to Lu-177 due to the very large cross-section for the (n, $\gamma$) reaction of Lu-176 (2090 b). This cross-section is the largest of any current radionuclide of medical interest and allows for very high specific activities compared to typical isotope productions using the direct activation route. The maximum specific activity of a material that is possible is known as the carrier-free (CF) specific activity and can be calculated as seen below. Where $\lambda$ is the decay constant, $N_A$ is Avogadro's constant, M is the molar mass and $t_{1/2}$ is the half-life.

$$SA_{CF} = \frac{\lambda N_A}{M} = \frac{\ln(2) N_A}{t_{1/2} M}$$

For Lu-177 the carrier-free specific activity is 4.1094 x $10^{12}$ Bq/mg or 111.06 Ci/mg. If a reactor with a very high thermal flux, >$10^{15}$ n/cm$^2$-s, such as the High Flux Isotope Reactor (HFIR) in Oak Ridge, Tennessee, or the SM-3 reactor in Dimitrovgrad, Russia is used, then specific activities as high as 50-65 Ci/mg can be achievable with a highly enriched target material. For research reactors with a medium thermal flux, ~$10^{14}$ n/cm$^2$-s, and target enrichment of 60-80% Lu-176 specific activities of 20-30 Ci/mg are achievable [5]. Despite being significantly lower than the CF specific activity these values are still sufficient for most TRT applications.

The direct route is capable of producing large quantities of Lu-177 of moderate quality. In addition, the processing steps post irradiation are much less complicated compared to the indirect route, only requiring the dissolving of the target with dilute mineral acid. The specific activity achievable using the direct method is proportionate to the thermal flux of the reactor being used. As a result, the direct method is best used with reactors with a relatively high thermal flux, unfortunately, this is not a possibility for many countries that do not possess high flux research reactors. Due to burnup and depletion of the target material there will exist a point of maximum activity at some point during the irradiation. After this point the specific activity of the product material quickly decreases. For irradiation with a high thermal flux, > $10^{15}$ n/cm$^2$-s, this peak activity is reached after approximately 4 to 5 days. For reactors with fluxes on the order of magnitude of $10^{14}$ n/cm$^2$-s, peak activity will be lower and may take anywhere from 20-40 days [6]. For some research reactors, such as HFIR, it is not possible, or at least very difficult, to remove targets during the middle of an irradiation cycle so it may not be possible to remove the target material at its peak activity. An additional drawback to the direct route is the production of the metastable isomer of Lutetium-177, Lu-177m. The production of this isomer only occurs through the direct route and has a much longer half-life than Lu-177 at 160 days. Although the ratio of Lu-177 to Lu-177m is very low at the end of burnup (EOB) at approximately 0.01-0.02 % this ratio grows larger and larger if the target is further irradiated and as the Lu-177 produced decays away. Medically Lu-177m is not a problem but may be an issue for countries with stringent waste policies as the patient's wastewater must be held in separate holding tanks for much longer periods to allow the Lu-177m to decay away to acceptable levels before discharging to the public sewer [5]. Overall,

the direct route benefits from a high production rate and simple chemical post processing but requires reactors with relatively high neutron fluxes, produces a product slightly contaminated with the metastable isomer Lu-177m and has a specific activity significantly lower than that of the theoretical possible CF specific activity.

Table 1.1. Neutron activation products of natural lutetium and ytterbium and nuclear characteristics of the product isotopes [1].

| Element | Target Isotope | Percent Abundance | σ (barn) | Activation Product | Mode of Decay | Half-Life $t_{1/2}$ | Decay Product |
|---|---|---|---|---|---|---|---|
| Lu | $^{175}$Lu | 97.40 | 16.7 | $^{176m}$Lu | β−, γ | 3.66 h | $^{176}$Hf |
| | | | 6.6 | $^{176}$Lu | β−, γ | $3.76\times 10^{10}$ y | $^{176}$Hf |
| | $^{176}$Lu | 2.60 | 2.8 | $^{177m}$Lu | β−, γ & IT | 160.4 d | $^{177}$Hf (78.6 %) |
| | | | | | | | $^{177}$Lu (21.4 %) |
| | | | 2090 | $^{177}$Lu | β−, γ | 6.64 d | $^{177}$Hf |
| Yb | $^{168}$Yb | 0.13 | 2300 | $^{169}$Yb | EC | 32.02 d | $^{169}$Tm |
| | $^{170}$Yb | 3.02 | 9.9 | $^{171}$Yb | Stable | - | - |
| | $^{171}$Yb | 14.22 | 58.3 | $^{172}$Yb | Stable | - | - |
| | $^{172}$Yb | 21.75 | 1.3 | $^{173}$Yb | Stable | - | - |
| | $^{173}$Yb | 16.10 | 15.5 | $^{174}$Yb | Stable | - | - |
| | $^{174}$Yb | 31.89 | 63 | $^{175}$Yb | β−, γ | 4.19 d | $^{175}$Lu |
| | $^{176}$Yb | 12.89 | 2.85 | $^{177}$Yb | β−, γ | 1.91 h | $^{177}$Lu |

***Indirect Route***

The second method for producing Lu-177 is the indirect route and involves irradiating Ytterbium-176 to produce Ytterbium-177 which subsequently decays to Lutetium-177, via beta decay, with a 1.91-hour half-life. This method, just like the direct route, has its advantages and drawbacks. Since the target material is a different chemical species than the product isotope this method allows for chemical separation of the Lu-177 that is produced. This allows for the highest achievable specific activity possible with results from 80 to 100 Ci/mg having been achieved [1][5]. In addition, since the product material is separated from the remaining target material the specific activity is not dependent on the neutron flux level, meaning that even with a low power research reactor very high purity Lu-177 with high specific activities can be produced. These very high

specific activities, able to be achieved with the indirect route, allow for additional types of TRT that require specific activities near the theoretical CF specific activity to be successful, as is the case in many radioimmunotherapy (RIT) applications [5]. Like the direct method, target enrichment is necessary to take full advantage of the best features of this production method. Typically, the target material used will be $Yb_2O_3$ for the same reasons the direct route uses $Lu_2O_3$. Natural Ytterbium consists of only 12.9% of the isotope Yb-176 with 31.9% being Yb-174. If the target material is not enriched to the highest amount of Yb-176 and the lowest amount of Yb-174 as possible then the Yb-174 will end up producing Lu-175 in the final product which will not be chemically separable from Lu-177, this will result in a significantly lower specific activity. If the indirect route is utilized with a target enriched in Yb-176 then the amount of the contaminate Lu-177m will be of indetectable levels. The irradiation of Yb-176 does not produce measurable amounts of Lu-177m. The only way for Lu-177m to be produced using the indirect route is for Yb-174 to be transmutated into Lu-175 which can then undergo two neutron captures, possibly becoming Lu-177m but most likely becoming Lu-177 instead. This side reaction is insignificantly small if the target material is enriched in Yb-176 and exposed to only a small to moderate neutron flux.

While the indirect route offers the prospect of producing NCA grade Lu-177 at up to 90% of the CF specific activity this is not without its difficulties and downsides. Yb-176 has a much smaller cross-section than that of Lu-176, 2.85 b versus 2090 b. This means that when the material has reached its saturation limit a very sizeable amount of the target material will still remain. This requires for the Lu-177 produced to be separated from the target and for the unburnt target material to be recovered and produced into a new target for subsequent irradiations. The production of this high-grade Lu-177 requires chemical separation of microscopic quantities of lutetium from macroscopic quantities of ytterbium, both of which share very similar chemical properties. The chemical separation step is easier said than done and is still a challenge for the industrial level production using this route. Multiple routes for chemical separation have been tested and proven but all require a multiple step purification process and produce a significant amount of radioactive waste material as a result. This complex chemical separation step also requires a significantly more advanced facility than that of the simple dissolution necessary when using the direct route. The production of Lu-177 using the indirect route is a feasible possibility for a much larger number of research reactors than the direct route and can ultimately produce a much higher-grade final

product with no impurities, however, this comes with a considerable increase in cost and complexity due to the secondary chemical processing steps required with this method. Both possible production routes for Lu-177 can be seen in Figure 1.3 below.

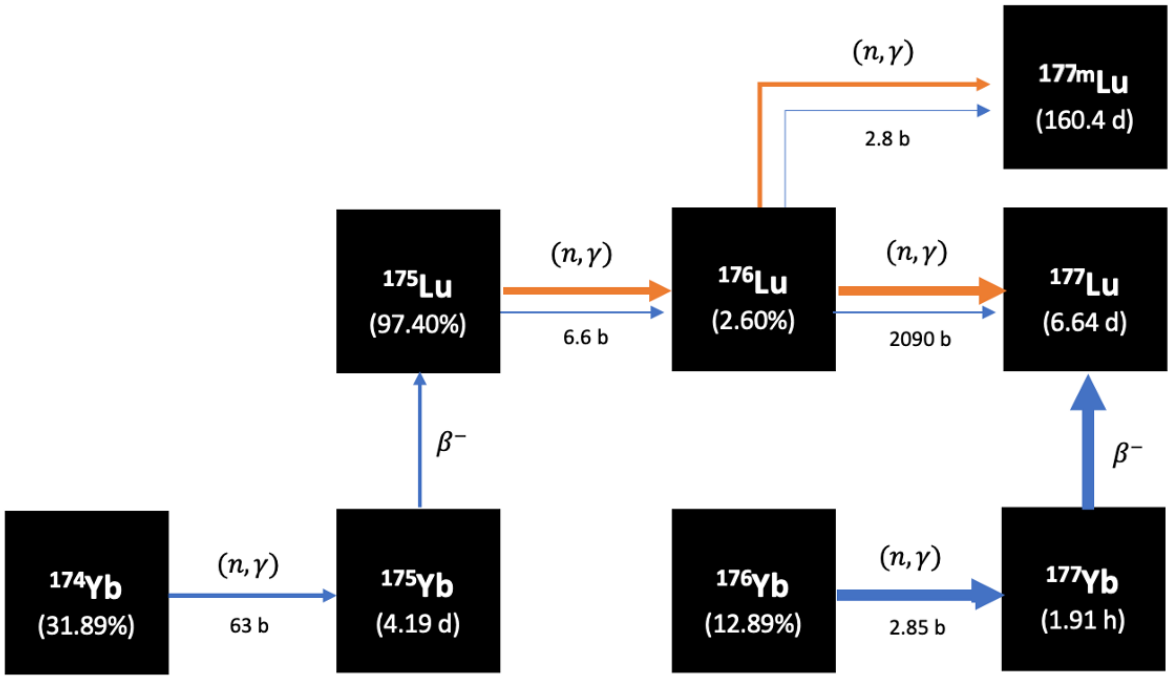


Figure 1.3. Main production pathways of the direct route (orange) and indirect route (blue) for Lu-177 production.

## 1.3 Limitations and Requirements

There are several limitations on what can be loaded into the PUR-1 core and for the maximum activity of material that can be produced at one time. In addition to this there are several limitations to what we can achieve due to the nature of PUR-1. Another constraint for this project is cost limitations, instead of being able to use ytterbium enriched in Yb-176, which is necessary to take advantage of the high specific activity afforded by the indirect route, natural ytterbium will be used instead. Additionally, after the irradiation of samples the dose rate needs to be low enough to allow for shipping to Niowave. This last requirement can be met with additional shielding if necessary.

The PUR-1 regulatory limits require that any change in core configuration or loading, for an experiment, be below 400 pcm of reactivity for either positive or negative reactivity changes.

To achieve this, it is necessary to simulate the experimental loadings using an MCNP model to determine the reactivity worth of each possible experiment. Additionally, the capsule containing the target material for irradiation must be double sealed. Niowave will be providing aluminum capsules that will fit in the irradiation ports with an internal rubber O-ring and an external thread cap so each capsule will have two seals. Lastly, the PUR-1 operating license limits the removal of anything from the core if the dose rate, measured at 30 cm, is over 1 R/hr. If the irradiation assembly is more radioactive than this allowed limit it will need to be placed back in the core and left to cool down until an acceptable level is reached. This may limit our ability to recover the target capsules, in a timely manner, if the dose rate is too high.

An additional limitation to the study is the 10 $kW_{th}$ power limit of PUR-1. The lower flux of PUR-1 limits the amount of activation that can be produced in target materials. This relatively low flux level could be countered by longer operating times but currently only one person is licensed for the operation of PUR-1 meaning that no longer than 6-to-8-hour irradiations can be performed at a maximum frequency of once per day. All of these factors and limitations limit the size and scope of this project to being a feasibility study rather than an attempt at actual production of medical grade Lu-177.

# 2. METHODS

## 2.1 PUR-1 MCNP Model

In order to ensure that all Committee on Reactor Operations (CORO) and Nuclear Regulatory Commission (NRC) requirements and guidelines are being upheld for the proposed experiments it was necessary to produce a high-fidelity Monte Carlo (MC) based neutronics model of PUR-1 in order to simulate and study the proposed procedures before actually performing them. In addition to ensuring that regulatory limits on reactivity insertion and dose rates were not likely to be violated, the MC model was also used for determining the optimum location for target irradiation as well as for predicting reaction rates of the isotopes of interest. The neutronics code MCNP6, developed by Los Alamos National Lab, was utilized for producing the model of PUR-1 [7]. From this MCNP6 model overall flux distributions, target reactivity worths and isotope reaction rates were directly determined. This model was also utilized in the verification of the reactor's power by simulating the results of a gold foil activation previously performed for power calibration purposes.

### 2.1.1 PUR-1 Description

PUR-1, as seen if Figure 2.1, is a pool-type research reactor built by Lockheed Nuclear Corporation in 1962. The reactor core is approximately 2 $ft^3$ in volume and is now licensed to be operated at 10 kW power. At 10 kW the maximum thermal flux achievable is approximately 4 x $10^{11}$ $n/cm^2$-s. The core sits on an aluminum grid plate at the bottom of a 17 ft, 6400-gallon pool of water which acts as coolant, moderator and shielding for the reactor. The large amount of water between the core and the surface allows for people to directly look at and observe an operating nuclear reactor without obtaining a significant dose of radiation. PUR-1 contains four power detectors each optimized for a different power range, in order to record the reactor power from startup to full power.

Figure 2.1. PUR-1 reactor, grid plate, coolant pool and detectors.

The active core region of PUR-1 consists of 16 fuel assemblies total, containing up to 14 fuel plates each for the 13 standard assemblies, and 8 plates each for the three special fuel assemblies containing control rod slots. Not all assemblies contain the maximum number of fuel plates with most assemblies having at least one dummy plate. The active core region is surrounded by 20 graphite block reflector assemblies clad in aluminum. Six of these reflector assemblies contain a half inch diameter aluminum tube which functions as an optional irradiation port. When not in use these irradiation ports contain a graphite slug to provide extra moderation and reflection into the core. Each fuel and reflector assembly contains a bottom plenum section that allows them to sit securely in the bottom grid-plate. Despite the core being only 6x6 assemblies the grid plate is 7 assembly locations tall and 11 locations wide allowing for great flexibility in the arrangement of the individual assemblies. The core also contains a 5 Ci Pu-Be neutron source which travels up and down in a 3-inch diameter tube at the side of the core and a half inch diameter stainless-steel drop-tube. The power is controlled by two borated stainless-steel safety control rods and one regulating control rod consisting of stainless steel with a void in the middle. The core geometry and location in the pool, as modeled in MCNP, can be seen if Figures 2.2 and 2.3 below.

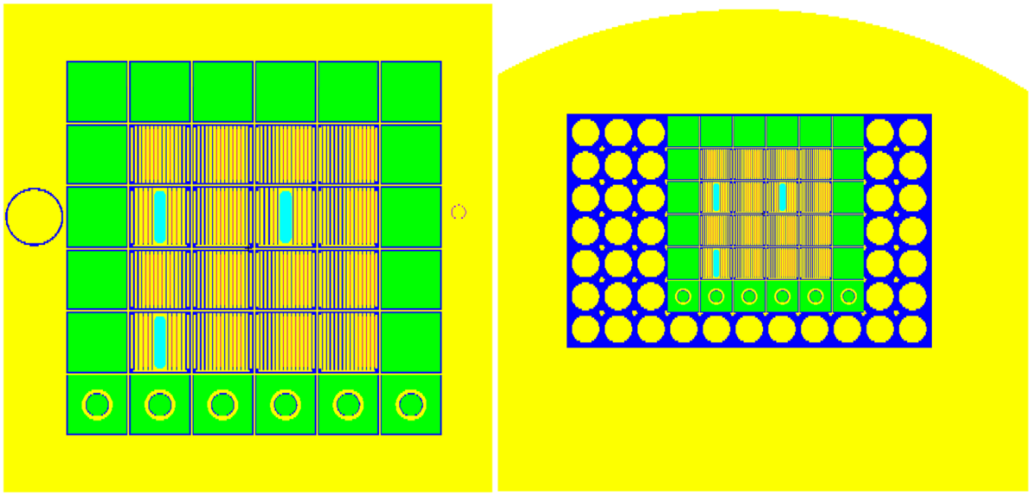

Figure 2.2. MCNP model geometry of core region (left) and core with grid-plate (right).

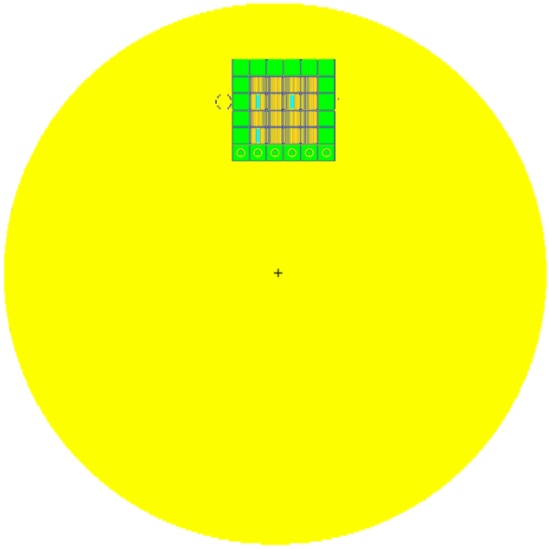

Figure 2.3. Orientation of core to pool region in x-y plane.

### 2.1.2 PUR-1 Core Composition

The first step in producing a reliable model of PUR-1 is to accurately reproduce the measured $k_{eff}$ value for an all-rods-out (ARO) case. To do this a very detailed and precise model of the core region is required. In 2007 PUR-1 was converted from HEU fuel to LEU fuel. Each fuel plate now consists of 0.02 inches of $U_3Si_2$-Al fuel meat clad in 0.015 inches of Al-6061 on

each side. The current fuel is enriched to 19.75% U-235 and each plate contains approximately 12.5g of U-235. The listed total mass of U-235 in the current core is 2369.96 grams, knowing that there are 190 plates in the current core configuration each plate is modeled as having 12.4735g of U-235 per plate [8]. Each plate in the standard fuel elements is spaced 3.71 mm apart while the special fuel element plates are spaced 5 mm apart. The spacing between the fuel plates are maintained by 6 spacer tabs on each side, distributed across the height of the assembly, for each plate. In addition to the fuel plates and spacers the aluminum assembly can is modeled in its exact geometry as defined in the original blueprint drawings. The plenum section of each assembly as well as the top tabs and cross bar are modeled as geometric approximations to the true shapes, for ease of modeling, but with the material volumes preserved in order to maintain the true fuel to moderator to structural material ratio in the core. The remaining assemblies modeled for the core consist of the graphite reflectors and the graphite irradiation port assemblies. The reflector assemblies consist of a simple block of graphite sealed by an aluminum cladding while the irradiation assemblies are the same with the addition of an aluminum tube down the middle of the center with a stainless steel and rubber stopper apparatus at the top. For this core configuration the irradiation port tubes are modeled with their graphite slugs inserted. The reflector and irradiation port geometries, as defined in the MCNP model, can be seen in Figure 2.4.

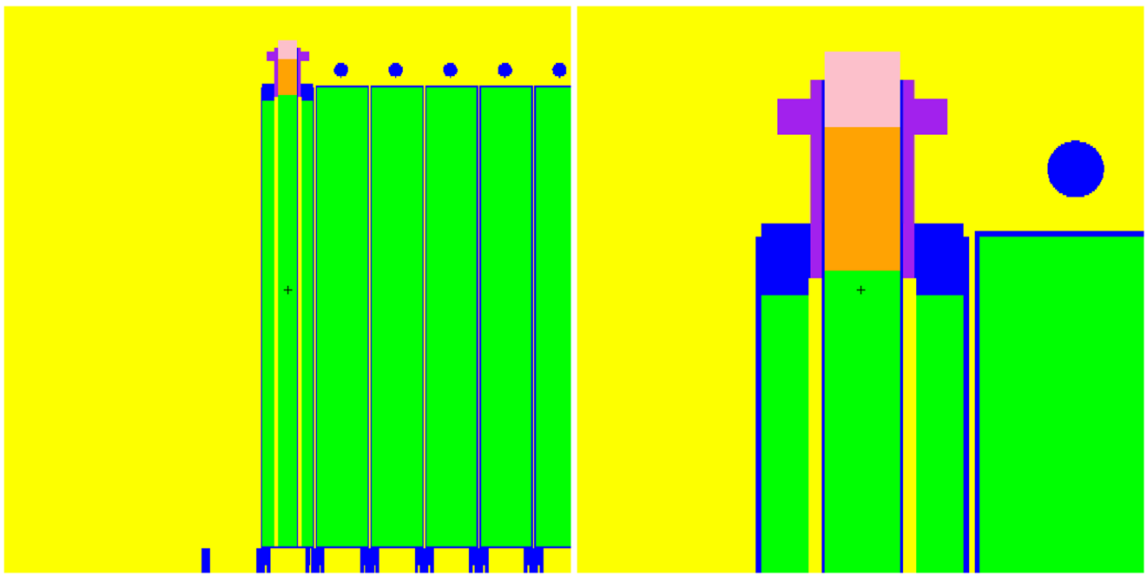

Figure 2.4. Y-Z plane cross-section of reflector and irradiation assemblies (left) and close up detail of irradiation port stopper (right).

### 2.1.3 ARO Core

With the core model completed with the exception of the source and control rods the first measurement of the multiplication factor ($k_{eff}$) of the system with ARO was performed and compared to measured values. The excess reactivity in PUR-1 with ARO is listed as being between 0.3% to 0.5% or 300 to 500 percent mille (pcm) reactivity, approximately. When the ARO case was run the resulting $k_{eff}$ was found to be 1.00749 +/- 0.00057, or approximately 749 pcm of excess reactivity. To adjust the core to have an excess reactivity of 300-500 pcm there were several parameters that could be adjusted. Both the density and boron impurity level of the graphite in PUR-1 are unknown as well as the amount of mineralization in the coolant water. The coolant water is obtained from city water that is run through a demineralizer. Even with the use of a demineralizer, radiation measurements show increased activity in the filters due to activation of minerals in the coolant water during prolonged runs. Initially the graphite in the core was modeled with densities and boron concentrations equivalent to that of modern-day reactor grade graphite, 1.79 g/cc and 0.1 ppm boron. However, due to the reactor being built in the early 1960's the density and purity of graphite used may very well be of a lesser quality. After several test cases a graphite density of 1.65 g/cc and a boron impurity of 0.88 ppm was selected which is close to the quality of graphite used in Chicago Pile 1 and 2 (CP1 and CP2) known as AGOT graphite which has densities of 1.60 to 1.71 g/cc and boron impurities from 2 ppm down to as low as 0.4 ppm [9]. Assuming the graphite used in PUR-1 is of similar quality to the AGOT grade graphite used in the Manhattan Project the density and boron impurity values assumed are reasonable. Secondly the original coolant material was assumed to be 100% pure light-water with no impurities at 20$^{o}$C. To model a more realistic case a boron concentration of 0.75 ppm was added to the water material in the MCNP simulation to account for dissolved minerals present in the coolant. Additionally, the average coolant temperature of PUR-1 was measured between 1999 and 2006 as being 26$^{o}$C [8]. The coolant temperature and density were changed in the model to reflect this. These changes resulted in an ARO $k_{eff}$ of 1.00447 +/- 0.00014 or approximately 447 pcm of excess reactivity, well within the range of the 300-500 pcm listed. Vertical and horizontal cross-sections of the fuel and spacer geometry can be seen in Figure 2.5.

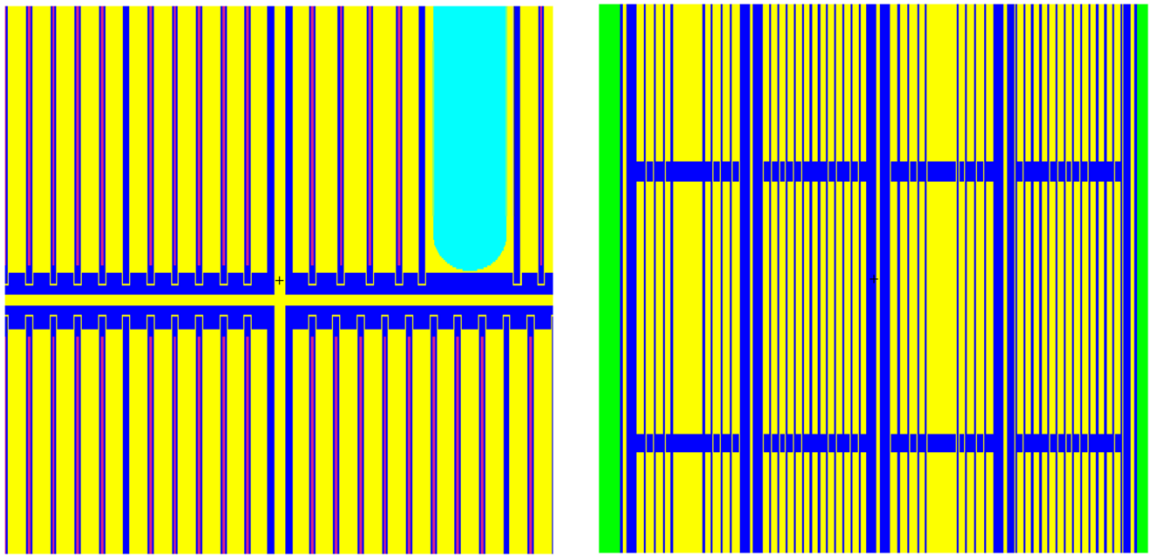

Figure 2.5. Fuel plate and fuel spacer details in x-y plane and x-z plane.

### 2.1.4 Control Rod Worths

With the successful completion of the ARO core case the next step was to model the three control rods of PUR-1; SS1 and SS2, which both consist of borated 304 stainless steel, and the RR control rod, or regulating rod, which consists of non-borated stainless steel with a central water gap. The exact boron concentration in rods SS1 and SS2 are unknown and as a result a series of guesses and checks were performed to try to fit the simulated rod worth curves as close as possible to the measured rod worth data. Blueprints for the RR rod were not available nor was data on the control rod's worth curve. As a result, the RR rod was modeled as being the same as the SS1 and SS2 rods and only configurations with the RR rod fully withdrawn are used for validation and verification with measured data. The reactivity worth for both SS1 and SS2 are known as well as their worth curves. In order to determine the appropriate boron concentration for the rods several MCNP runs were performed, one with the SS1 rod fully inserted and the SS2 rod fully withdrawn and vice versa, then this was repeated with a different boron concentration until the simulated full rod worths were as close to the measured rod worths as possible. This was found to occur at approximately 3100 ppm boron. From here MCNP runs with one rod withdrawn and the other withdrawn 0 cm, 10 cm, 20 cm 30 cm etc. were performed for both rods. The resulting rod worth curves predicted by MCNP can be seen plotted against the measured rod worth curves in Figure 2.6. One measured critical rod height (CRH), with the RR rod fully removed was recorded which

allows for the same rod positions to be simulated to see how close to critical that configuration is when modeled. The measured CRH was with SS1 and SS2 both at 50.92 cm and RR fully withdrawn (62.5 cm). This case was then simulated and the resulting $k_{eff}$ was 0.99996 +/- 0.00017 or within 4 pcm of critical.

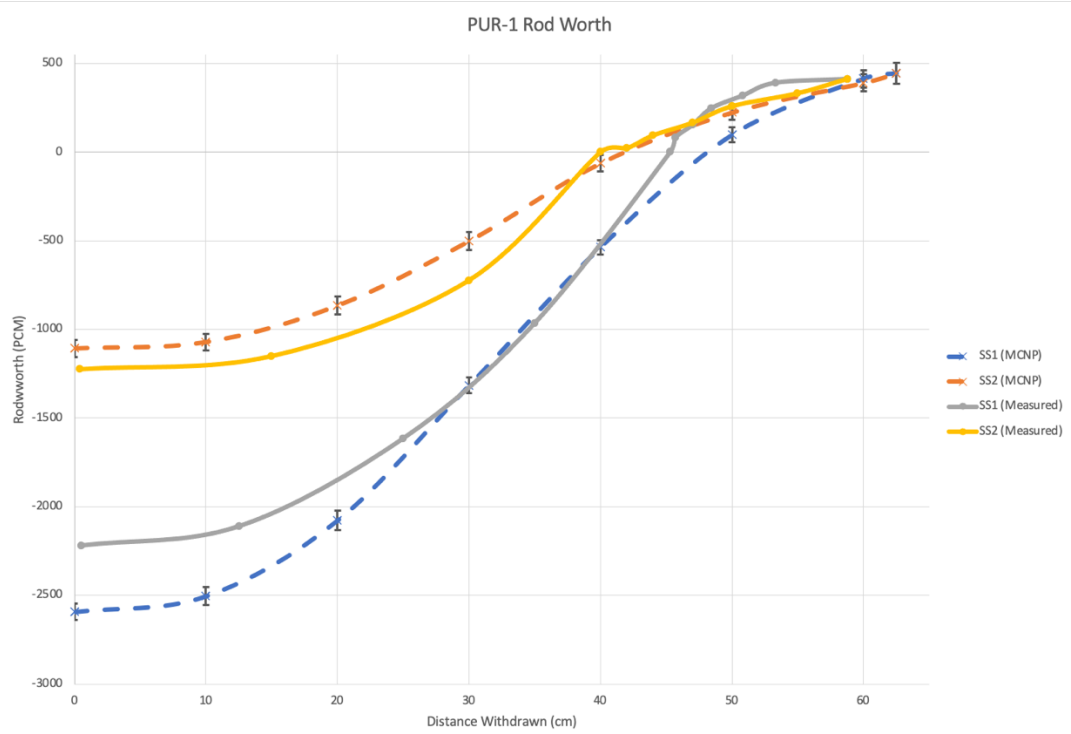


Figure 2.6. Measured versus simulated control rod worth curves for SS1 and SS2.

## 2.2 Optimal Loading Location

With a high-fidelity base model of PUR-1 it was then possible to determine the optimum location for irradiating a $Yb_2O_3$ target capsule by determining which irradiation port contains the greatest thermal flux. In order to do this 10 separate MCNP runs were performed, one for each irradiation port and four to test the effects if one irradiation port was moved to one of the other three reflecting sides. For these 10 simulations one of the graphite slugs was removed from the irradiation port and a small stainless-steel capsule containing the target $Yb_2O_3$ material was modeled in the middle of the irradiation port at the centerline of the core. The remaining region where the graphite slug used to be was modeled as air. The flux in the target material is able to be determined, for each case, by specifying a simple F4 tally in the cell containing the $Yb_2O_3$ material.

The F4 tally is described as being a "track length estimate of cell flux" and can be further customized by specifying multiple energy bins for the tally [10]. To determine the thermal flux in the ytterbium oxide containing cell an F4 tally was used with three energy bins, one for the thermal range, one for the epithermal range and one for the fast flux range. The results of these tallies are in units of neutrons per square centimeter per second per source particle. To convert from tally results to a flux in n/cm$^2$-s for a given power level, the following equation was utilized.

$$\phi\left[\frac{n}{cm^2 s}\right] = \frac{P[W]\bar{\nu}\left[\frac{n}{fission}\right]\phi_{F4}}{1.6022 \times 10^{-13}\left[\frac{J}{MeV}\right] w_f \left[\frac{MeV}{fission}\right] k_{eff}}$$

The results of these ten trials can be seen in Figure 2.8 and show that the irradiation assembly in location G6 has the highest thermal flux at 1.625E11 n/cm$^2$s and is the best location for the irradiation of the ytterbium oxide target. Based on these MCNP runs it was decided to utilize the G6 irradiation port for all experimental irradiations moving forward. The grid designation for all assemblies can be seen below in Figure 2.7.

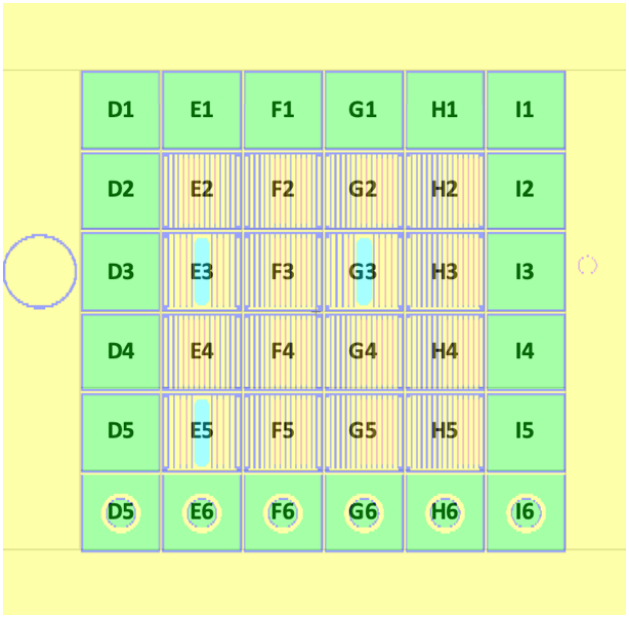


Figure 2.7. Grid number designation of each assembly.

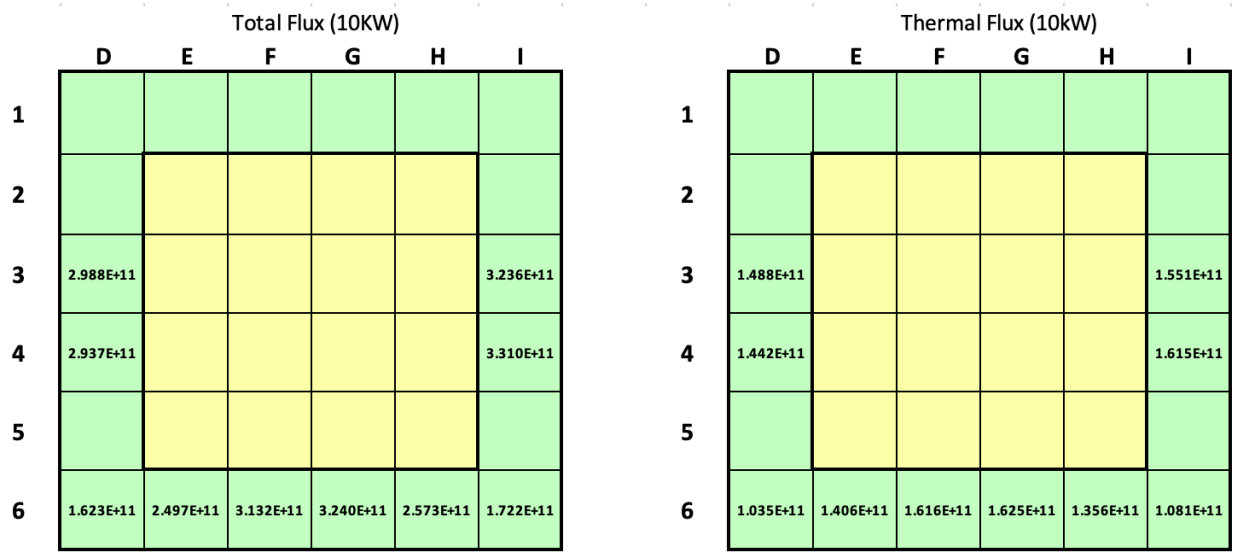


Figure 2.8. Predicted total and thermal flux in target capsules using MCNP F4 tallies.

## 2.3 Reaction Rate Tallies

MCNP was also utilized to predict reaction rates for each ytterbium isotope present in the target material. However, to do this is was necessary to first generate cross-section data files for each ytterbium isotope as the ENDF-VII library currently used by MCNP lacks cross-sections for ytterbium. With the help of my professor Dr. Yunlin Xu, the code NJOY was able to be utilized to produce MCNP cross-section data files for all-naturally occurring Ytterbium isotopes. With the help of the Engineering Computer Network (ECN) staff at Purdue the MCNP data files were appended to include those for Ytterbium. With the necessary cross-sections installed, the reaction rates for each ytterbium isotope were determined by using multiple F4 tallies on the cell containing the ytterbium oxide target material in the model, one for each Yb isotope. Each F4 tally was modified by multiplying it by the number density of the isotope in question, in units of #/cm-b, and the microscopic cross-section for (n, $\gamma$) reactions in a material specified as being the pure isotope of interest, this can be seen in the first two lines of Figure 2.9 The flux in cell 3097, which contains the ytterbium oxide, is taken and multiplied by the number density of the Yb-168 isotope in the target material. This is then multiplied by the microscopic (n, $\gamma$) cross-section for material 168 which is specified in the material deck as being isotopically pure ytterbium-168. This F4 tally and series of tally multipliers gives us the number of (n, $\gamma$) reactions that occur per source particle.

To find the reaction rate for a given power level these results can be converted using the previous equation used to calculate the real predicted flux from the F4 tally flux.

```
f4:n   3097
fm4   (6.93179E-06 168 102)  $Yb-168 reaction rate
f14:n   3097
fm14  (1.66308E-04 170 102)  $Yb-170 reaction rate
f24:n   3097
fm24  (7.82082E-04 171 102)  $Yb-171 reaction rate
f34:n   3097
fm34  (1.19678E-03 172 102)  $Yb-172 reaction rate
f44:n   3097
fm44  (8.85619E-04 173 102)  $Yb-173 reaction rate
f54:n   3097
fm54  (1.75473E-03 174 102)  $Yb-174 reaction rate
f64:n   3097
fm64  (7.08968E-04 176 102)  $Yb-176 reaction rate
```

Figure 2.9. Tally card for determining reaction rates.

## 2.4 Isotope Production and Decay Modeling

With the MCNP predicted reaction rates of each isotope of interest it was then possible to model the production and decay of the different product isotopes produced from radiative capture reactions (n, $\gamma$). Since the production rate of product isotopes is dependent on the decay or radiative capture rate of other isotopes and their initial amounts, the system of equations produced describing each isotopes production and destruction is a series of partial differential equations. These equations describing the chain of nuclear transformation that occur is a type of Cauchy problem for the system of balance equations whose form can be seen below [6].

$$\frac{dN_i}{dt} = \sum_{j \neq i} R_i^j N_j(t) - R_i N_i(t), \quad i = 1, \dots, x;$$

$$N_i(0) = N_{i0}, \qquad i = 1, \dots, x$$

In these equations $N_i(t)$ is the number of nuclei of type 'i', $R_i^j$ is the rate of decay of the j$^{th}$ nuclide into the i$^{th}$ nuclide per nuclei j, $R_i$ is the rate of burnup and decay of the i$^{th}$ nuclide per nuclei i and 'x' is the number of nuclides in the system [6]. To solve this system of equations two different methods were employed, one was through the use of a MATLAB script developed to solve a simplified set of the equations seen above using a finite difference strategy and the second was through the implementation of the burnup code module known as ORIGEN, from the SCALE code system, to simulate the burnup and the resultant product isotopes produced.

### 2.4.1 MATLAB Model

The first method developed, to solve the chain of nuclear transformation that takes place when natural Ytterbium is irradiated, is a MATLAB script written to utilize the reaction rates determined from MCNP tallies. With the reaction rates of each isotope along with reactor power, ytterbium mass and irradiation durations as inputs, the amounts, activities, and dose rates of each product isotope as a function of time are able to be determined. These determinations are performed by making several assumptions. The first assumption is that depletion of target material and destruction of product isotopes from radiative captures is negligible due to the relatively low thermal flux produced in PUR-1 and the short irradiation time periods, less than a day. Therefore, in this model $N_i(0) = N_{i0} = N_i(t)$ for nuclides whose number density is not equal to zero at the start of irradiation and that the contribution to $R_i$ from radiative capture is zero for nuclide whose number density is equal to zero at the start of irradiation. With these simplifications the number densities of the four main radioactive product isotopes of interest, Yb-169, Yb-175, Yb-177 and Lu-177, are solved for using a first order finite differencing scheme with one-minute timesteps. A sample of the simplified finite difference method for Yb-177 and Lu-177 can be seen below.

$$dN_{Yb177} = -\lambda_{Yb177} N_{Yb177}(t-1) + \phi(t) R_{Yb177}$$
$$N_{Yb177}(t) = N_{Yb177}(t-1) + dN_{Yb177}$$
$$A_{Yb177}(t) = \lambda_{Yb177} N_{Yb177}(t)$$
$$N_{Yb177}(0) = 0, \qquad A_{Yb177}(0) = 0$$

and

$$dN_{Yb177} = -\lambda_{Lu177} N_{Lu177}(t-1) + A_{Yb177}$$
$$N_{Lu177}(t) = N_{Lu177}(t-1) + dN_{Lu177}$$
$$A_{Lu177}(t) = \lambda_{Lu177} N_{Lu177}(t)$$
$$N_{Lu177}(0) = 0, \qquad A_{Lu177}(0) = 0$$

In these equations $R_i$ is the radiative capture reaction rate of the parent isotope calculated from the MCNP tallies. For short irradiation times and relatively low flux levels this simplified system is able to accurate predict the number density and activities of the product radioisotopes of interest. This MATLAB script is also set up in such a way to allow for a varying flux value with time to allow for multiple startup and shutdowns or other non-constant flux scenarios.

### 2.4.2 ORIGEN Model

The second method utilize to solve the systems of production and decay is to use ORIGEN to model the burnup of an ytterbium oxide target. The Oak Ridge Isotope Generation code (ORIGEN) is a module of the SCALE code package developed at Oak Ridge National Laboratories and is used to calculate the time dependent concentrations and activities of large numbers of radionuclide produced from transmutation, fission, and radioactive decay [11]. Typically, ORIGEN is used in conjunction with a 2D or 3D lattice code such as Polaris or Triton to predict fuel burnup between timesteps but can be used as a standalone code to predict the burnup and production of various isotopes in a target material. To simulate the burnup of the ytterbium oxide target and subsequent growth and decay of the products of interest it was first necessary to generate a 252-group neutron spectrum of PUR-1 to input into the ORIGEN input. To do this an F4 tally of the cell containing the target material was again performed. This time applying energy tallies specifying each of the 252 energy groups so that a 252-energy group spectrum would be produced at the end of the calculation. This MCNP produced neutron spectrum can be seen in Figure 2.10.

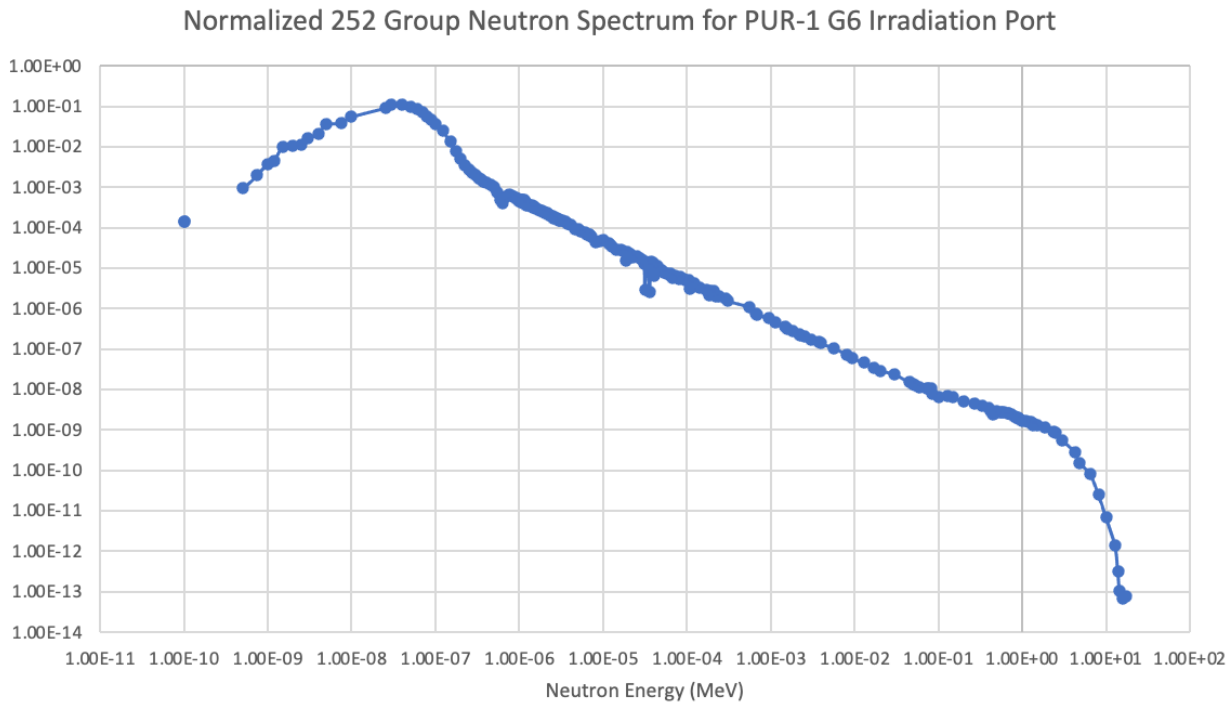


Figure 2.10. Normalized 252-Group neutron spectrum for the G6 irradiation port of PUR-1.

Due to the relatively small size of the cell containing the ytterbium oxide target along with the small bin width of the energy groups MNCP simulations with a very large number of particles and active cycles were required to produce a neutron spectrum with sufficiently small uncertainties for each energy group. With this neutron spectrum specified in the ORIGEN input along with the mass of each element in the target, the flux level expected, and the durations of the burnup and cooldown periods, the production and decay of all the various nuclides are able to be calculated. The resulting concentrations and activities of all isotopes produced are stored in a .f71 file which can then be plotted and viewed using Fulcrum. This method is meant to verify the results of the simplified model produced using MATLAB.

# 3. EXPERIMENT

The overall purpose of this experiment for both Niowave and Purdue is not to produce medical grade lutetium-177 but to instead, for Purdue, to test the feasibility of isotope production in PUR-1 with our new power upgrade, and for Niowave to produce test material to test and refine their chemical separation techniques for possible future productions. As a result, natural ytterbium would be utilized rather than a much more costly target material enriched in Yb-176. While the specific activity of the lutetium we produce will be much lower than desirable due to the production of Lu-175 from the significant amount of Yb-164 in the target it will allow us to test our simulation and calculation techniques used to predict the concentrations and activities of the product isotopes and to extrapolate the possible results if enriched targets were used in the future for longer irradiation periods.

## 3.1 Gold Foil Power Calibration

The first step to prepare for the irradiation of the Ytterbium targets is to calibrate the power level of PUR-1. To do this a series of gold irradiation experiments were performed. This calibration technique is based on a 1981 dissertation by Gary Harms where the overall flux profile of PUR-1 was determined with numerous activation experiments of either gold or copper wire at many different locations throughout the core [12]. From this data the rate of activation for a small gold foil, placed in the half-inch drop tube at the reactor midplane, is related to the power level of the reactor. For this one location in the reactor the rate of gold activation to reactor power was found to be 2.93 $\mu$Ci/100W-g-min [12].

The power of the reactor is calibrated at several different energies, first at 1% power then at 5%, 10%, 25% and 50% before the last calibration is performed for 100% of its rated power. For each energy level calibration, a small gold foil is placed in a specially made acrylic rod which has a space in it for the gold foil to sit. This rod acts as a spacer in the drop tube and aligns the gold foil to the midplane of the core. Once the gold is in place in the acrylic rod the reactor is brought to the desired power level and the rod is then quickly dropped down the drop tube. The reactor is kept level at this power level for anywhere from one to three minutes at which point the acrylic rod, containing the gold is quickly pulled out, effectively removing it from the flux almost

instantly. Since the gold is irradiated for a very short time, relative to its half-life, a linear relationship between irradiation time and activity can be assumed to exist to exist.

Once the gold is removed from the reactor it is then placed on an acrylic holder plate containing a Cs-137 and Ba-133 check source and placed in front of a Canberra HPGe detector to obtain a gamma spectrum and number of counts from the gold foil, as seen in Figure 3.1 below.

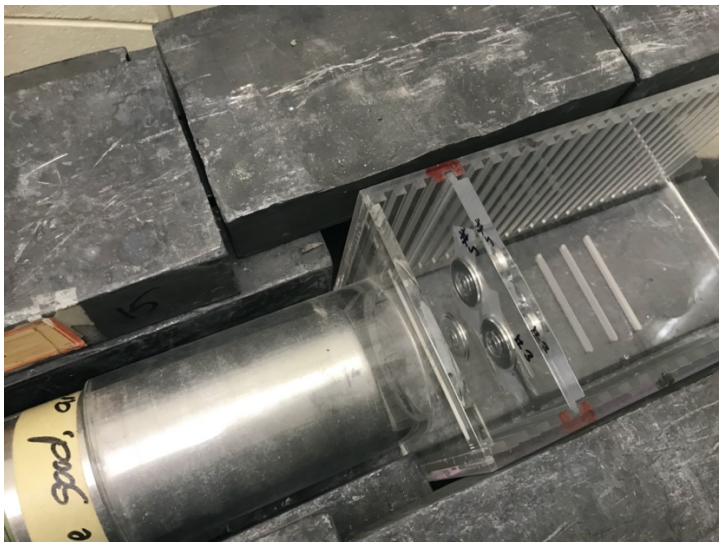

Figure 3.1. HPGe detector and source geometry.

The purpose of the check sources is to be able to determine the detector efficiency as a function of energy only since all three gamma sources are effectively in the same geometry as each other relative to the detector. With the detector efficiency, gold mass, irradiation time, delay time, measurement time and counts detected it is possible to determine the real activity of the sample. From this activity the true power the reactor was operating at during the irradiation can be determined with the use of the constant determined in the 1980's. From the ratio of the measured power to the calculated power the four different detectors in the core are adjusted to match the calculated power. If the calculated power and measured power are within 10% then the next calibration step is performed. If they are not within 10% then that power step's calibration is reperformed.

$$A_{0,198} = \frac{\dot{C}_{198} \cdot e^{\lambda_{198} t_d}}{B.R._{198} \cdot \epsilon_{411}} \qquad P = \frac{A_{0,198}}{18.1 \cdot t_{irr} \cdot m_{Au198}}$$

## 3.2 Target Irradiation

With the reactor power calibration successfully completed the preparation for the irradiation of the ytterbium oxide targets was able to begin. Originally it was planned to perform four small scale irradiations with an increasing amount of ytterbium oxide each time in order to ensure that neither the dose rate limit or reactivity insertion limits would be exceeded. Each sample of ytterbium oxide was loaded into a HDPE capsule which is then loaded into a roughly 3-inch by ½-inch diameter aluminum irradiation capsule, known as a rabbit. The first and smallest sample to be irradiated consisted of 0.258g of $Yb_2O_3$, however due to delays this sample was left loaded in the irradiation port for a significant period of time. Although the reactor was at zero power the PuBe source was in its inserted position. Due to this a small but measurable amount of irradiation of the sample material occurred due to neutrons produced from the source propagating in the subcritical system. To produce results that could more easily be compared with simulations it was decided to start with the next smallest sample, sample #2 which contained 2.554g of $Yb_2O_3$.

### 3.2.1 Sample #2 Irradiation

Sample #2 was loaded into the core by first removing the entire irradiation assembly from the G6 location. This is done with a specialized hooking mechanism attached to a 20-foot pole. The hooks are lowered into the pool and engaged when they are securely attached to the docking rods of the assembly. Once secured the assembly is lifted to the surface of the pool at which point the activity of the assembly is measured to ensure that it is less than 1 R/hr at 30cm. Once the dose rate was measured and ensured to be below this limit the assembly was lifted over the side of the pool structure and placed down on the floor of the lab. From here the irradiation port tube was rotated 90 degrees to unlock it from the rest of the assembly and removed. With the irradiation tube removed from the remainder of the assembly the rubber stopper at the top of the tube was removed and the graphite slug withdrawn and placed behind lead shielding. Into the tube three dummy rabbits, containing nothing except air, were loaded into the tube to act as spacers, followed by the rabbit containing the HDPE vial with the ytterbium oxide. Following the loading of the irradiation port the rubber stopper was placed back on the tube and the tube reinserted back into the irradiation assembly. The irradiation assembly was then reattached to the loading hook tool and lowered back into the pool and placed back into its original position.

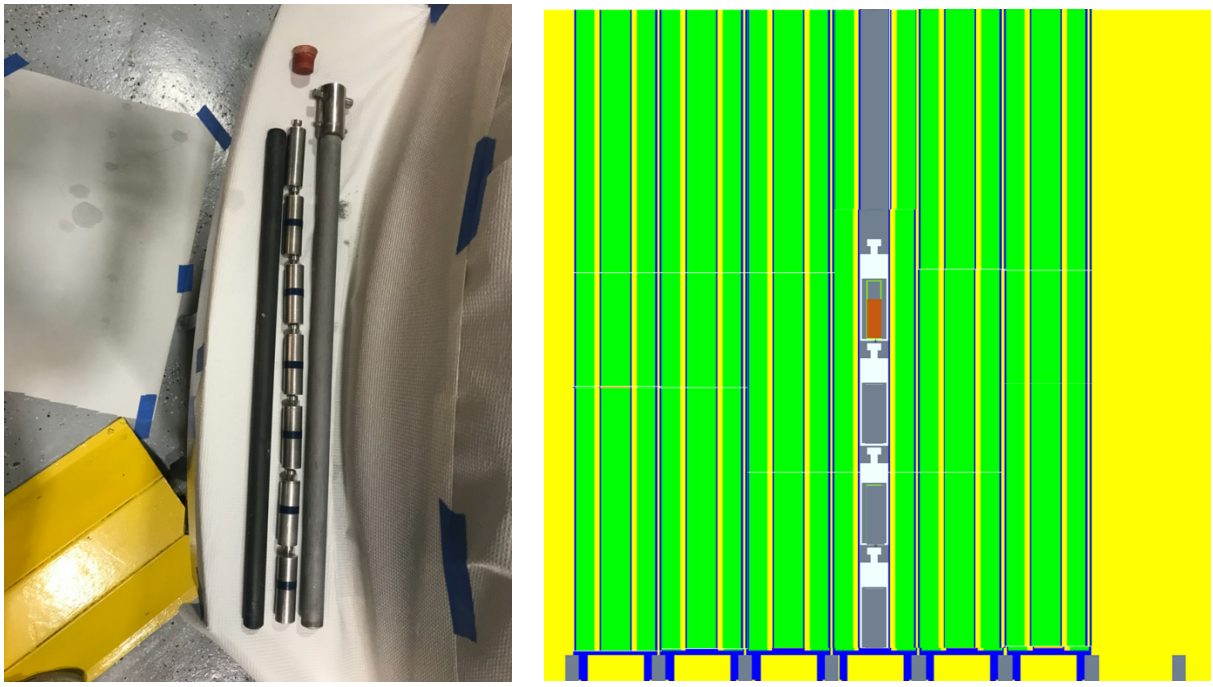

Figure 3.2. Graphite rod, irradiation rabbits and irradiation port tube (left) and MCNP model of experiment geometry (right).

With the now loaded irradiation facility placed in its original position of G6 it was then possible to begin the first irradiation trial. For this irradiation it was decided to only irradiate the material for a short amount of time at a lower power in order to get a baseline of what dose rate we should expect from the following higher power and longer duration trials. The SS1 and SS2 control rods were then set to the previous known critical positions and the RR rod was raised until power change rate was level at zero. The power of this first run was approximately 12 watts and the sample was irradiated for approximately 22 minutes. At the end of this irradiation, with the SS1 and SS2 control rods still at their previous known critical positions the RR rod was lowered to the position at which was once its critical height when the graphite rod was in the G6 irradiation port. The negative change rate of the power was then recorded, and the control rods were lowered to end the first irradiation experiment.

With the value of the negative change rate measured, when all three control rods were at their original critical position, it is possible to determine the reactivity worth of the core change from having a graphite rod in G6 to having three dummy capsules and a fourth one containing the

ytterbium oxide. The change rate is inferred to the reactivity worth through the use of the inhour equation seen below.

$$\rho = \frac{\Lambda}{T_p} + \sum_{i=1}^{6} \frac{\beta_i}{1 + \lambda_i T_p}$$

Where $\rho$ is reactivity in %k/k, Λ is the mean neutron generation time, $T_p$ is the reactor period and $\beta_i$ and $\lambda_i$ are the 6 group delayed neutron fractions and precursor decay constants. With the reactivity worth of this new configuration known we then decided to determine the reactivity worth of the first sample containing 0.258 grams in order to determine the worth of the ytterbium oxide alone to see if the higher mass loadings would still be under the reactivity change limit of 400 pcm. Once all control rods were fully inserted the G6 irradiation assembly was again removed from the core and its dose rate again recorded before fully removing it from the water. The irradiation port tube was again removed and the rabbit containing the ytterbium oxide removed for further evaluation. In its place the aluminum rabbit containing the smaller 0.258g sample was inserted. The irradiation assembly was then reassembled and inserted back into the core to its original position.

After a short delay the capsule containing the 2.455g loading was transported to a proximal HPGE detector and a 120-minute gamma spectroscopy measurement was taken followed by a 60-minute background measurement. During this measurement the reactor was brought to critical again, this time with the 0.258g sample inserted. Once a level power was achieved the RR rod was again lowered to the CRH recorded from when the graphite slug was still located in G6. From the reactivity calculated from this negative change rate and the reactivity calculated sample #2 there was strong confidence that we would not come close to exceeding the 400 pcm limit with the fourth, and largest, sample of 9.362g. For this reason, it was decided to skip the third sample of the series and go straight to the fourth sample for a short full power irradiation. Once the reactor was fully shutdown the G6 irradiation assembly was again removed, and the dose rate checked at the surface. Once confirmed to be below the dose rate limit the assembly was again fully removed from the pool and the irradiation port tube removed. The capsule containing the 0.258g sample was then removed and the capsule containing the fourth and largest prepared sample of 9.362g

was inserted in its place on top of the three dummy spacers. The G6 irradiation assembly was then reassembled and placed back in its original position in the core.

### 3.2.2 Sample #4 Irradiation

The irradiation of the 9.362g sample began like the previous two in which the SS1 and SS2 control rods were set to their original CRHs and the regulating rod raised until a positive change rate was recorded. The regulating rod was then slowly lowered until a change rate of zero was achieved. Based on the position of the RR rod it was certain that even with this higher mass loading of ytterbium oxide that we were still well below the reactivity insertion limits and that it was safe to proceed. The regulating rod was again raised from this critical position and the power was allowed to increase to approximately 90% of the core's rated power or 9 kW. Once at this power level the RR rod was reinserted back to its previous critical position to maintain the power at that level. The sample was irradiated at this power for approximately 20 minutes at which point the reactor was shut down with a manual scram. Roughly 10 minutes later an attempted was made to remove the G6 irradiation assembly from the pool but a dose rate of over 1 R/hr at 30 cm was recorded. The assembly was placed back into its original position and allowed to cool overnight. At this point it was decided to further irradiate the fourth sample of 9.362g to confirm the effects of multiple irradiations on Lu-177 production. A plan for five additional irradiations for 6 hours each, one each day starting the following day was decided upon.

The following day, after examining the two-hour gamma spectrum taken the previous day, it was decided to perform a 24-hour measurement with the HPGe detector in order to produce a more pronounced Lu-177 peak for a more accurate measurement. This measurement was started in the early afternoon. Following this, preparations for that day's irradiation of the fourth ytterbium oxide sample were started. Once all reactor checks were completed the power was slowly brought up to 85% power, or 8.5 kW. The reactor was kept at this level for approximately 4 hours and 10 minutes. Throughout the period of this irradiation the RR rod had to be regularly adjusted to account for the increase in coolant and core temperature in order to maintain criticality. Before shutting down entirely the RR rod was set back to its original critical position, measured at the start of the 9kW irradiation. From this recorded negative change rate, the moderator temperature coefficient of reactivity is able to be determined. Following this the control rods were gang lowered to shut down the reactor. Throughout the irradiation period the temperature of the pool water was

being monitored and it was noticed that the temperature change rate was greater than what was expect for a power of 10 kW. At this point it was decided to cease reactor operations until a further analysis could be performed.

The G6 assembly was left to cool for two days at which point the assembly was removed from the pool and the capsule with sample #4 containing the 9.362g of $Yb_2O_3$ was removed. Due to technical difficulties with the HPGe detector in the nuclear engineering laboratory a sufficient gamma spectrum was not able to be recorded before the sample was shipped off three days later. A sufficient gamma spectrum of this sample was able to be recorded at the Niowave facilities eleven days after the end of the irradiation of the sample. An approximately one-hour measurement was performed with their HPGe detector along with a calibration measurement using a europium-152 source. This data was then provided to us from Niowave thanks to Chad Denbrock and Jeremy Pike.

# 4. RESULTS

Throughout the duration of the calibrations and experiments performed on PUR-1 for this project the data from all sensors monitoring PUR-1 were recorded in real time and available for analysis. This recorded data includes everything from the ion chamber detectors used for determining power level and control rod positions to the pool coolant temperature and the air pressure in the reactor room. With all of this data at our disposal for analysis interesting trends can be noticed that were not possible before switching to a fully digital operating and recording system. For the duration of these experiments the operating data for the reactor is available. In addition to this, the dose rates and gamma spectrographs for the second and fourth ytterbium oxide capsule were recorded and able to be analyzed to confirm our irradiation models. With both the highly detailed power data from the reactor and the measured count rates for the two irradiation trials it is possible to determine the amount of each product isotope produced.

## 4.1 Pool Temperature Analysis

To better understand the results of the two irradiation trials performed it is first necessary to analyze the unexpected pool temperature data results obtained during the four-hour irradiation of capsule number 4 at 85% power. Using the simplified equation seen below it was estimated beforehand that the pool water temperature should rise approximately 0.356ºC per hour of operation at full power, 10 kW.

$$\Delta T = \frac{Pt}{mc_p}$$

In this equation $m$ is equal to the mass of the 6400 gallons of water in the pool, $c_p$ is the specific heat of water, $P$ is the power the reactor is operating at and $t$ is the amount of time the reactor is at that power. In Figure 4.1 below, the power reported by three of the four channels can be seen plotted against the thermocouple readings of the pool water temperature for the roughly 4-hour irradiation of capsule 4. The recorded temperature at the start of the irradiation period was 25.5ºC and by the end of the 4 hours the water temperature was recorded as being 27.7ºC. This represents a temperature change of 0.55ºC per hour. Plots of the coolant temperature change rates during and after irradiation can be seen in Figures 4.2.

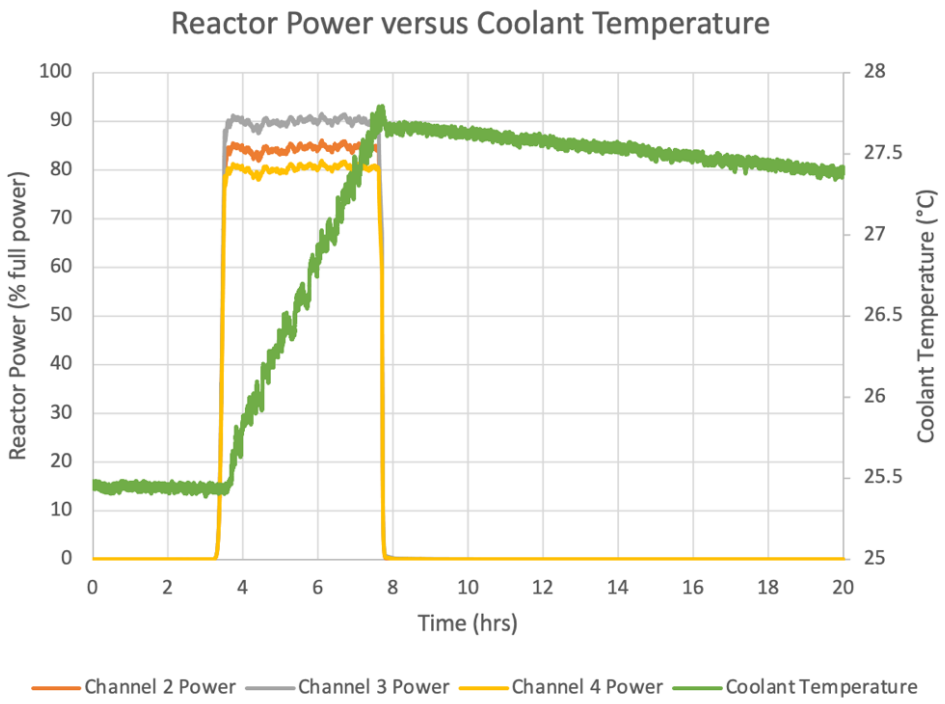


Figure 4.1. Reactor power and pool temperature for the irradiation of capsule 4.

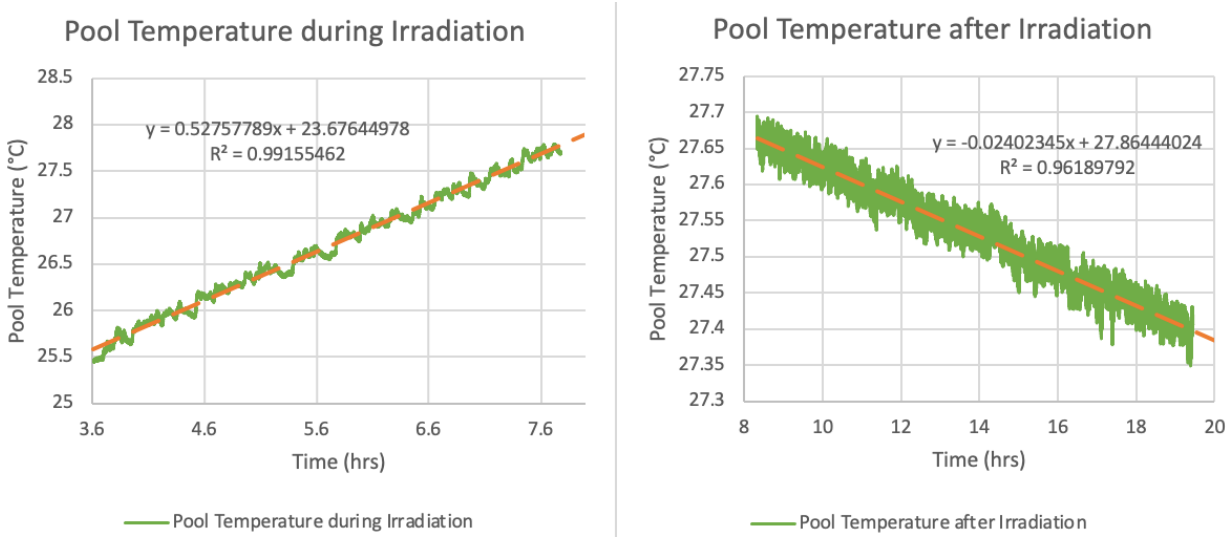


Figure 4.2. Pool temperature during irradiation and after irradiation.

With a closer analysis of the coolant temperature data, it can be seen that there is a slight delay from when the reactor is powered up to when the coolant temperature begins to rise followed by a very rapid increase in temperature. This rapid increase lasts for approximately a couple of

minutes and then the rate of temperature change follows a near linear pattern. At the end of irradiation, when the reactor is shutdown, there is a relatively large drop in temperature followed by a near linear decrease in pool temperature. Taking the line of best fit for both linear sections of temperature change we obtain a value of 0.526ºC/hr for the rate of temperature increase during irradiation and a value of -0.0238ºC/hr for the rate of temperature decrease after shutdown. This later value can be considered to be the rate of heat loss occurring from the reactor pool at all times and therefore can be added to the temperature increase rate to find the total increase rate for if the system was adiabatic. This results in a value of 0.5498ºC/hr. Assuming the system is adiabatic and isothermal then this temperature increase rate would suggest that the power the core was operating at was closer to 15.4 kW than 8.5 kW.

In order to gain more confidence in the results of this simplified model it is necessary to determine if the assumptions of an isothermal and adiabatic system are accurate to reality. The temperature data comes from a single thermocouple located several feet above the core. This may explain the delay in the temperature change rate at the beginning of the irradiation and the rapid drop in temperature at shutdown. However, it is unknown if the water in the pool undergoes a sufficient amount of circulation and mixing to assume that the bulk pool temperature is the same as the temperature registered by the thermocouple over the core. The majority of the mixing in the pool is assumed to be due to the 30 gallon/min pump used to circulate water through the demineralizer. To determine this, a computational fluid dynamic (CFD) simulation of PUR-1 is necessary. Thanks to the help of Dr. Ran Kong at Purdue University a 3D CFD model of PUR-1 and its coolant pool was simulated using the software ANSYS Fluent. This model can be seen in Figure 4.3. To simulate this transient first a steady-state flow with the energy equation turned off is developed. Once a steady-state flow has developed the energy equation is turned on and the heat transfer to the flow determined. Since there is no cooling of the water the inlet temperature of the core is set to the pool bulk temperature. Several simulations at different powers from 10 kW to 15.5 kW were performed. The results of these trials can be seen in Figure 4.4.

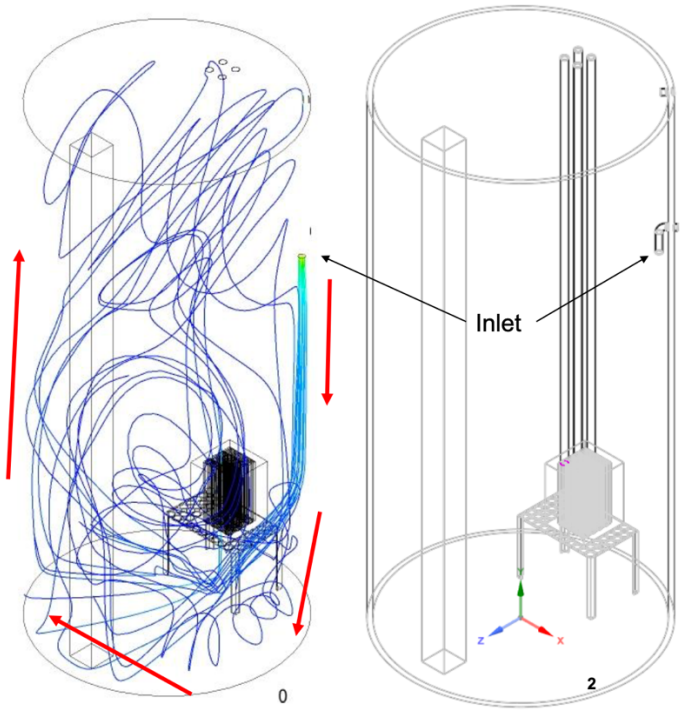


Figure 4.3. ANSYS Fluent model of PUR-1 curtesy of Dr. Ran Kong.

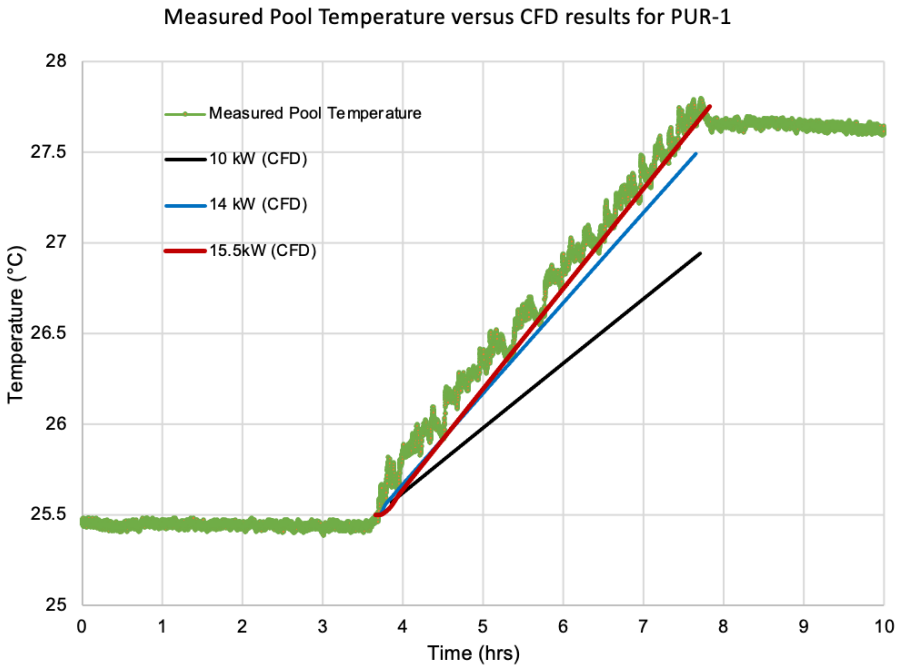


Figure 4.4. Measured pool temperature versus CFD model results curtesy of Dr. Ran Kong.

Comparing the results of Dr. Kong's Fluent simulation results for PUR-1 to the measured thermocouple data it can be seen that the CFD suggests that the operating power of the reactor was definitely greater than 10 kW and somewhere close to 15.5 kW based on the slope of the measured data compared to the slope of the CFD results. This supports the results obtained with the previous assumptions that the pool water was essentially isothermal. Both the simple analysis of the change rate of the measured data and the more accurate CFD results suggest that the reactor was running at 15-15.5 kW for this period of time rather than the 8.5 kW suggested by the average of the three power channels. This implies that the power calibration previously performed was off by 70-80%. Determining the true power the core was operating at during the irradiations of the two target capsules is necessary for determining the accuracy of the two irradiation models developed to simulate the concentrations and activities of the product isotopes.

## 4.2 Gold Activation Calibration Number

A third method for determining the power level of the core is to reproduce the gold activity to core power calibration constant using the MCNP model of PUR-1 and to see if it matches the original value used. In order to reproduce the calibration constant, used in the power calibration procedure, the base MCNP model of PUR-1 was taken and a small 0.5 cm by 0.5 cm by 0.0021 cm gold foil weighing 0.010143g was simulated along with the acrylic holder rod in the center of the drop tube. The gold foil is modeled as being in line with the centerline of the core. It is not possible to measure the radial distance the drop tube is from the edge of the reflector assemblies although a clear gap can be seen between the two. It is assumed that the inner edge of the drop tube is located 2 cm from the edge of the reflector assemblies for modeling purposes. With the gold foil and acrylic spacer modeled a MCNP run was performed with multiple tallies to determine both the reaction rate in the gold foil and the fission rate in all cells containing fuel.

The first tally for the (n, $\gamma$) reaction rate is specified with an F4 tally for the cell containing the gold foil and by multiplying this tally by the microscopic cross-section of gold. This calculation results in the number of (n, $\gamma$) reactions per cm$^3$ per source particle. Multiplying this by the volume of the cell, containing the gold foil, results in the number of (n, $\gamma$) reactions per source particle.

$$\phi_{F4}\sigma_{Au197}V_{Au} = 3.6291 \times 10^{-7} = (n.\gamma)\ reactions\ per\ source\ particle$$

An F4 tally was also applied to the sum of all the fuel plate containing cells. This flux tally was then multiplied by the fission cross-section of the fuel material and by the total volume of all the cells containing fuel. This results in the number of fission reactions per source particle.

$$\phi_{F4}\sigma_f V_{fuel} = 0.29797 = fission\ reactions\ per\ source\ particle$$

With these two tallies provided from the MCNP output it is then possible to determine the ratio between the activity of the gold foil and the power level of the reactor. The energy released per fission event is approximately 200 MeV converting this to joules and multiplying this by the number of fissions per source particle gives us 9.548x10$^{-12}$ J or watt-seconds per source particle.

$$200\left[\frac{MeV}{fission}\right] * 1.602 \times 10^{-13}\left[\frac{J}{MeV}\right] * 0.29797\left[\frac{fission}{Source\ Particle}\right] = 9.548 \times 10^{-12}\left[\frac{W-s}{Source\ Particle}\right]$$

The number of (n, $\gamma$) reactions per source particle can then be divided by the number of watt-seconds per source particle to obtain the number of Au-198 atoms produced per watt second.

$$\frac{3.6291 \times 10^{-7}\left[\frac{(n.\gamma)\ reactions}{Source\ Particle}\right]}{9.548 \times 10^{-12}\left[\frac{W-s}{Source\ Particle}\right]} = 3.8008 \times 10^{4}\ \left[\frac{Au-198\ atoms}{W-s}\right]$$

This value can then be multiplied by 60s and divided by the mass of the gold foil to give the number of Au-198 atoms produced per W-g-min.

$$3.8008 \times 10^{4}\ \left[\frac{Au-198\ atoms}{W-s}\right] * \frac{60s}{0.010143g} = \ 2.2483 \times 10^{8}\left[\frac{Au-198\ atoms}{W-g-min}\right]$$

Lastly multiplying this number by the decay constant of Au-198, 2.98x10$^{-6}$ s$^{-1}$, dividing this number by 37000 Bq/$\mu$Ci and finally multiplying this by 100 gives us the ratio of the activity to power in the original units of $\mu$Ci/100W-g-min

$$2.2483 \times 10^{8} \left[\frac{Au - 198\ atoms}{W - g - min}\right] * \frac{2.98 \times 10^{-6}[s^{-1}]}{37000\left[\frac{Bq}{\mu Ci}\right]} * 100 = 1.8095\ \left[\frac{\mu Ci}{100W - g - min}\right]$$

This activity to power ratio constant, calculated from MCNP tallies, is approximately 40% less than the current value used for power calibration, 2.93 $\mu$Ci/100W-g-min. The results from this test calculation suggest that if the reactor power was calculated using the 2.93 value then when you are at what you believe to be a power of 9 kW you would actually be at a power of 14.57 kW according to the constant derived from the MCNP model results. Two additional MCNP simulations were run due to the uncertainty of the drop tube position relative to the core. One test case 1.6 cm from the reflector assembly face and one 2.4 cm from the reflector assembly. For the 1.6 cm case the constant was calculated as being 1.9617 $\mu$Ci/100W-g-min and for the 2.4 cm case 1.6250 $\mu$Ci/100W-g-min. These results can be seen plotted in Figure 4.5. This shows that even a small change in position has a great impact on this constant due to the rapid rate at which the flux dies away outside of the reactor core. Without knowing the precise location of the gold foil both radially and axially this method of calibration may have too great of a degree of uncertainty to be of great use.

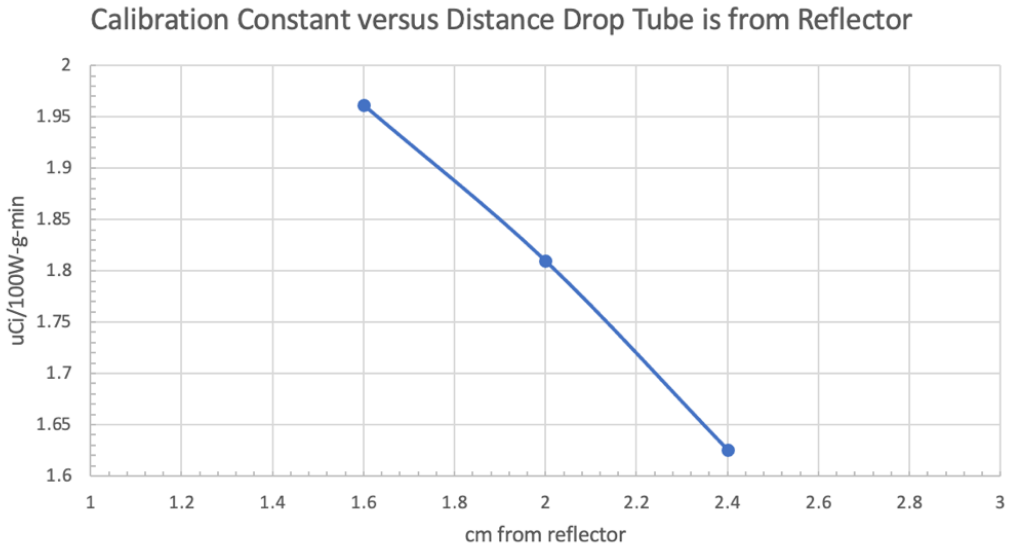


Figure 4.5. Calibration constant versus drop tube location.

## 4.3 Low Power Irradiation

### 4.3.1 Gamma Spectrum

The first sample to be irradiated was the 2.455g sample, capsule #2. This sample was irradiated, in the G6 irradiation assembly, for approximately 22 minutes at 12 W of power. Two hours after irradiation the sample was placed in front of a Canberra HPGe detector and a two-hour gamma spectrum was recorded. After analyzing the results of this spectrum, it was found that this was not a sufficient measuring window to detect a sizeable peak from the isotope of interest, Lu-177. The following day, 27 hours after removal from the core, a 24-hour long gamma spectrum was recorded. With this longer recording time a significant Lu-177 peak was obtained. Several interesting observations can be made from both gamma spectrum. In the 2-hour spectrum, recorded shortly after irradiation, the higher energy peaks, 1080 keV and 1241 keV, of Yb-177 can be seen however, by the following day when the 24-hour spectrum was recorded these peaks and the dominant 150 keV peak are no longer detected. This is due to the relatively short 1.9-hour half-life of Yb-177. A second point of interest between these two spectra is the very dominant peak seen at 846.7 keV in the 2-hour measurement but not the 24-hour measurement the following day. It was determined that this peak is due to Mn-56 which has only a 2.6-hour half-life. This radionuclide was produced from neutron activation of the Mn-55 present in the aluminum alloy used for the irradiation capsules. With peaks from all four of the radioisotope products of interest captured between the two gamma spectrum measurements it is possible to determine the true activities of each.

Table 4.1. Common gamma energies and branching ratio of the four radioisotope products of interest.

| **Yb-169** | | **Yb-175** | | **Yb-177** | | **Lu-177** | |
|---|---|---|---|---|---|---|---|
| **E (KeV)** | B.R. (%) | E (KeV) | B.R. (%) | E (KeV) | B.R. (%) | E (KeV) | B.R. (%) |
| **63.12** | 43.62 | 396.33 | 13.1 | 150.4 | 18 | 208.37 | 10.41 |
| **197.96** | 35.93 | 282.52 | 6.13 | 1080.2 | 5.08 | 112.95 | 6.23 |
| **177.21** | 22.28 | 113.81 | 3.87 | 1241.8 | 3.07 | 321.32 | 0.2186 |
| **109.78** | 17.39 | 144.86 | 0.672 | 121.62 | 3.05 | 249.67 | 0.1997 |
| **130.52** | 11.38 | | | 138.62 | 1.22 | | |

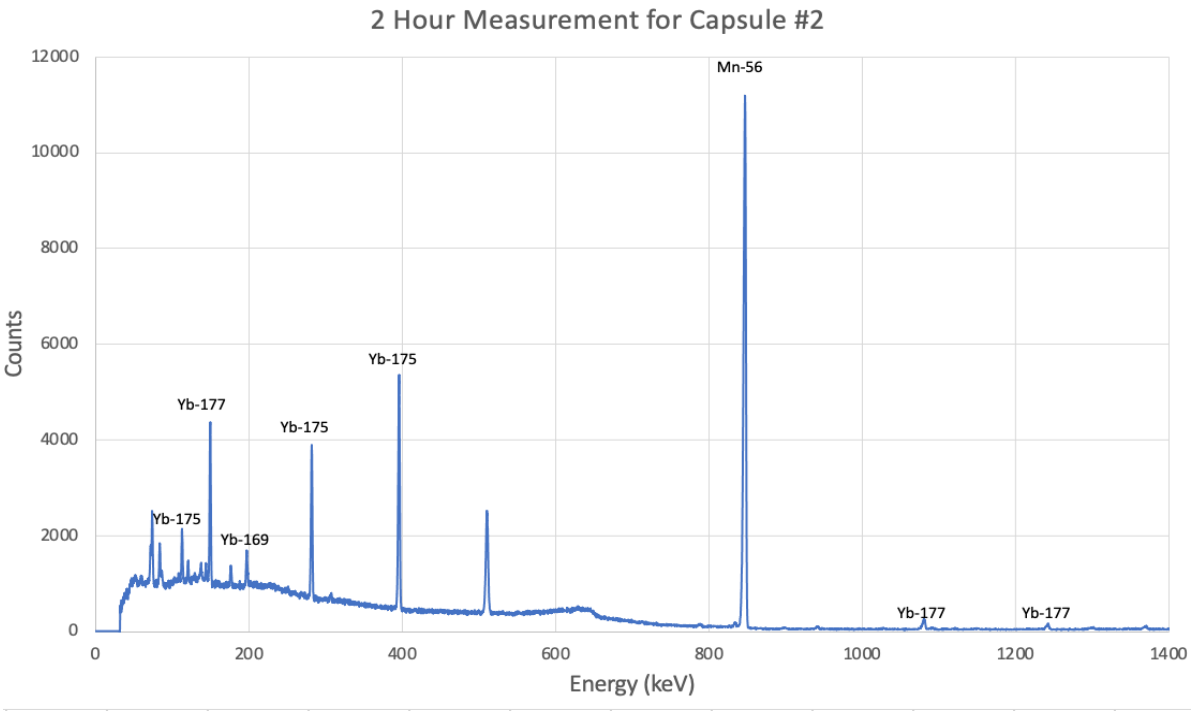


Figure 4.6. 2-hour gamma spectrum of capsule #2.

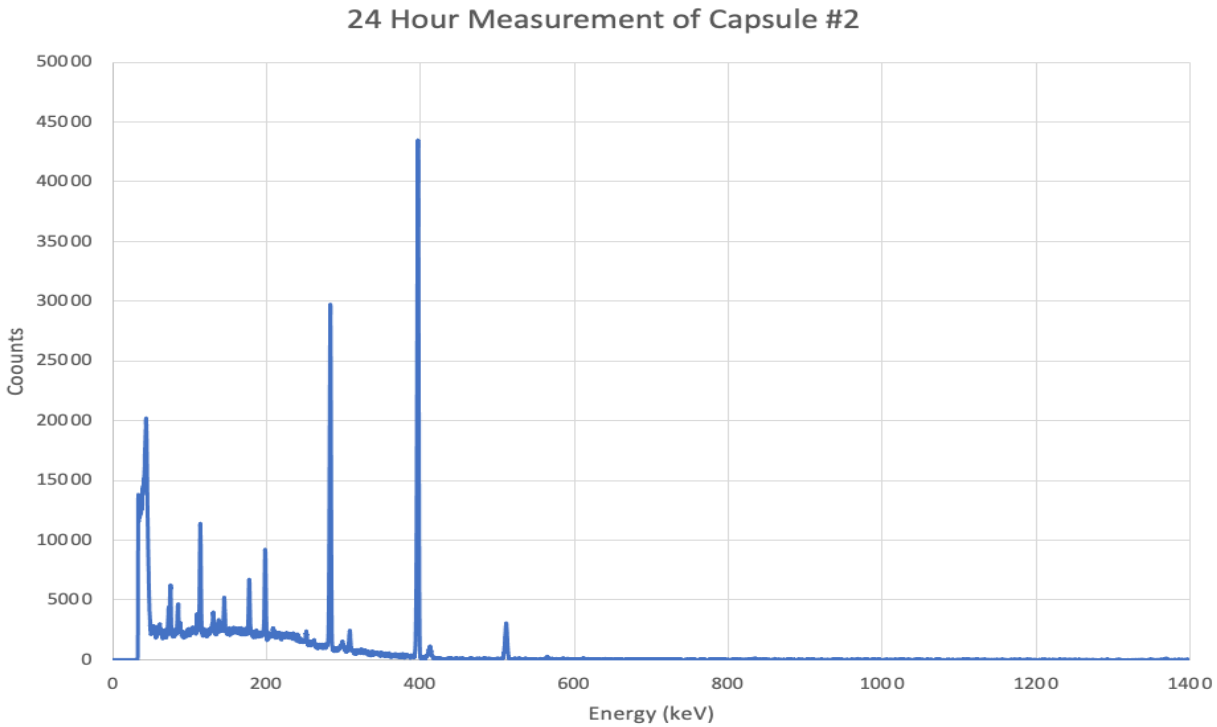


Figure 4.7. 24-hour gamma spectrum of capsule #2.

### 4.3.2 Detector Efficiency

In order to determine the true activity, of each isotope in the sample, it is necessary to account for numerous factors such as the detector efficiency as a function of both distance and energy, the branching ratio of the isotope's decay, the gamma attenuation through different materials to the detector, and the decrease in activity that occurs during the measurement window. To account for the detector efficiency, two sources of known activity were placed in the same location where the capsule was measured so that both measurements would have the same source to detector geometry. The two known sources were a Cs-137 and Ba-133 source. The spectrum, from these two sources, provides five peaks ranging from 276 keV to 661 keV that can then be plotted to produce a detector energy curve as a function of energy only. For most HPGe detectors the energy efficiency curve for this energy range can be well approximated using an exponential curve. This exponential trend will stay true for energies ranging from approximately 150 keV to 1 MeV. When an exponential line of best fit is applied to the efficiencies of the known sources a fairly good fit is obtained with A= 0.002271 and b= -0.003296 for the equation y = Ae^bx, where y is the detector efficiency and x is the energy of the gamma peak. This detector efficiency curve can be seen in Figure 4.8.

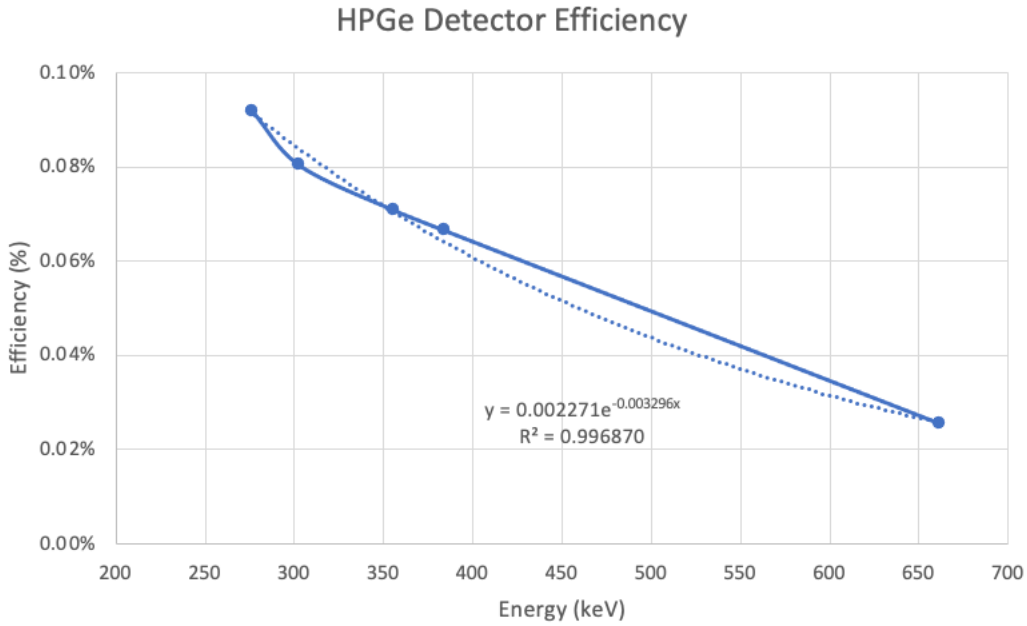


Figure 4.8. HPGe detector efficiency curve.

### 4.3.3 Count Corrections

The first step in determining the true activity was to determine the net counts of each peak. This was done by selecting the beginning and end point of each peak and summing the counts of all the energy bins between these two points. Then the background counts between these two points are determined by taking the average of the left endpoint bin and right endpoint bin and multiplying this by the number of bins the peak occupies. By subtracting the background counts from the gross number of counts under the peak the net detected counts is obtained.

Table 4.2. Peaks of interest for each isotope as well as measured net counts.

| Isotope | E (KeV) | B.R. (%) | t_1/2 (d) | lambda (/hr) | Gross Counts | Background Counts | Net Counts |
|---|---|---|---|---|---|---|---|
| **Lu-177** | 208.37 | 10.41 | 6.443 | 0.0044825 | 41777 | 35838 | 5939 |
| **Yb-177 *** | 150.4 | 18 | 0.079625 | 0.3627143 | 46274 | 22473 | 23801 |
| **Yb-175** | 396.33 | 13.1 | 4.185 | 0.0069011 | 507124 | 9758 | 497366 |
| **Yb-169** | 197.96 | 35.93 | 32.018 | 0.0009020 | 125848 | 52417 | 73431 |

* Data and measurement times for Yb-177 are from the 2-hour measurement since no discernable peaks could be obtained in the 24-hour spectrum. All data for the other three isotopes are from the 24-hour spectrum.

With the net counts of each peak determined, corrections for the isotope's branching ratio, the detector's efficiency at that energy, gamma attenuation though the ytterbium oxide and aluminum capsule, as well as for the change in activity throughout the measurement can then be accounted for. The four equations below are used to determine the current activity, at the end of the gamma spectrum measurement, from the measured number of net counts. In these four equations $\epsilon(E)$ is the detector efficiency for that particular energy gamma, $\gamma_{atten}$ is the gamma attenuation factor of all the materials combined, in this case it was assumed the capsule was a point source and that the aluminum thickness was equal to the capsule wall thickness and that the thickness of the ytterbium oxide was equal to the radius of the capsule. Lastly, $C_{ct}$ is the count-time correction factor and accounts for the difference in activity at the beginning of the measurement and the end of the measurement. With short gamma spectrum measurements for isotopes with relatively long half-lives this correction is not necessary, and it can be assumed that the activity at the end of measurement is roughly equal to the activity at the beginning and that therefore, the current activity is just equal to the average counts per second over the measurement window. In our case the

measurement times are equal to a significant fraction of the half-lives of the isotopes being measured, therefore this correction factor is needed.

$$Current\ Activity\ (Bq) = \frac{Net\ Counts * C_{ct}}{B.R * \epsilon(E) * t_m * \gamma_{atten}}$$

$$C_{ct} = \frac{\lambda t_m e^{-\lambda t_m}}{1 - e^{-\lambda t_m}}$$

$$\epsilon(E) = 0.002271 e^{-0.003296 * E(keV)}$$

$$\gamma_{atten} = e^{-\mu_{Al} x_{Al} + \mu_{Yb} x_{Yb} + \mu_o x_o}$$

### 4.3.4 MATLAB and ORIGEN Modeling

With the activities of the isotopes at the end of the gamma spectrum measurement calculated, the irradiation of sample #2 was simulated using both the simplified MATLAB model and with ORIGEN to determine if either give good agreement to the measured data. The ORIGEN model utilizes the 256-group neutron spectrum determined from the F4 tally of the cell containing the $Yb_2O_3$. The MATLAB model utilizes the reaction rates determined from the F4 tallies specified in the input of the MCNP simulation. For the MATLAB model these reaction rates are based off of the cross-sections generated for MCNP using ENDF-VIII data to fill in the missing cross-sections for the naturally occurring Ytterbium isotopes. From the recorded power history of PUR-1, seen in Figure 4.9, the average power for the steady-state region was found to be approximately 12 W. Additionally, the total burnup was found to be equal to 0.004434 kw-hrs. To approximate this power history as a step-function a burnup period of 22 minutes at 12.0927 W was chosen and input into both models. With the reaction rates, neutron spectrum, burnup duration and power level input the last input need for the models was the cooldown period which was set equal to 52 hours to see what the predicted activities are at the end of the gamma spectrum measurement, 51 hours and 19 minutes after the end of the irradiation. The measured/calculated activities and those predicted by both MATLAB and ORIGEN can be seen below in Figures 4.10 & 4.11 as well as in Table 4.3.

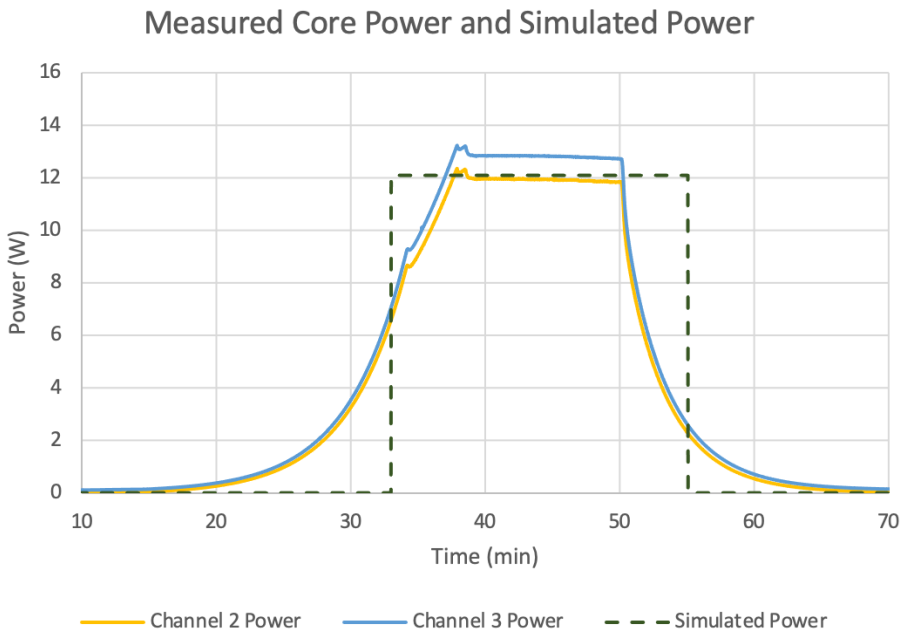


Figure 4.9. PUR-1 recorded power history and simulated power history for capsule #2.

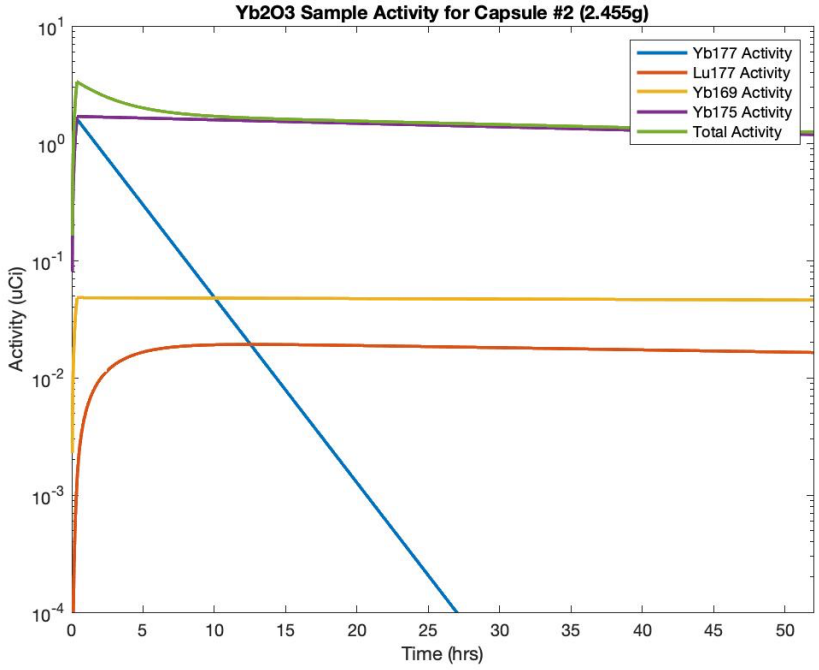


Figure 4.10. MATLAB simulated activities for capsule #2.

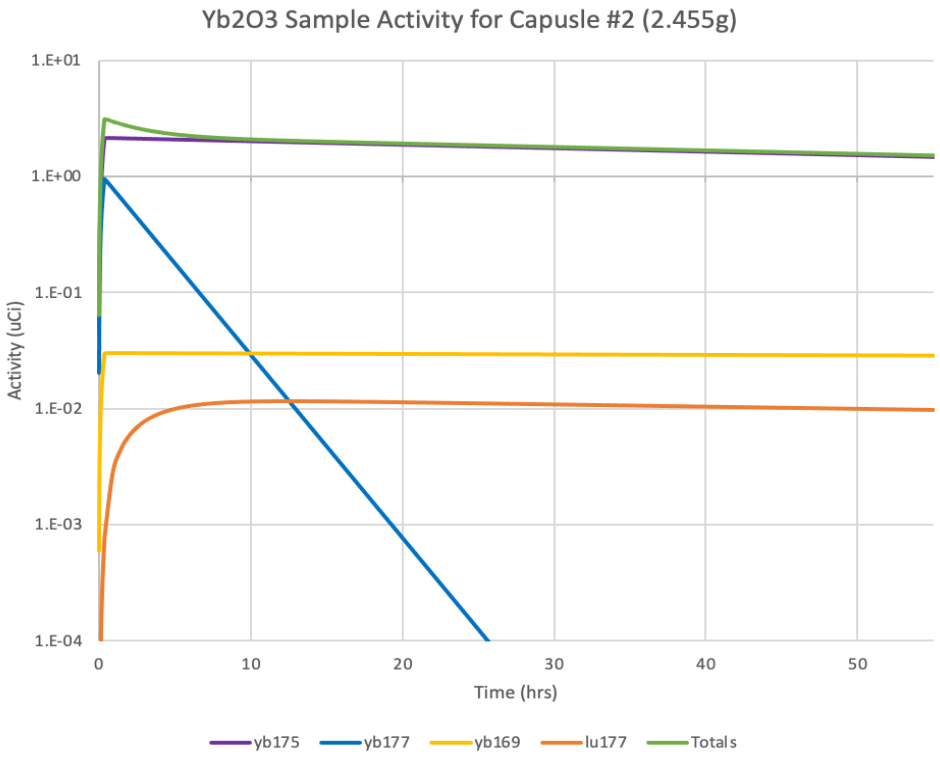


Figure 4.11. ORIGEN simulated activities for capsule #2.

Table 4.3. Measured and simulated isotope activity.

| Isotope | Current Activity ($\mu$Ci) | MATLAB Current Activity ($\mu$Ci) | MATLAB % difference | ORIGEN Current Activity ($\mu$Ci) | ORIGEN % difference |
|---|---|---|---|---|---|
| **Lu-177** | 0.02943 | 0.01646 | -44.08% | 0.00935 | -68.23% |
| **Yb-177 *** | 0.91442 | 0.42829 | -53.16% | 0.25800 | -71.79% |
| **Yb-175** | 2.19241 | 1.18997 | -45.72% | 1.51000 | -31.13% |
| **Yb-169** | 0.07436 | 0.04599 | -38.15% | 0.02860 | -61.54% |

* Data and simulations for Yb-177 are for the 2-hour measurement since no discernable peaks could be obtained in the 24-hour spectrum. All data and simulations for the other three isotopes are for the 24-hour spectrum.

It can be seen that both the MATLAB model and the ORIGEN model produce similar results. The main difference between the two models may be due to the different cross-section data used by ORIGEN. Like MCNP, ORIGEN currently utilizes ENDF-VII data for its burnup cross-sections. When a cross-section does not exist in ENDF-VII ORIGEN then checks the JEFF3.0/A neutron activation files for cross-sections. For ytterbium isotopes the JEFF3.0/A neutron activation files do have cross-sections and therefore this is the data set used by the ORIGEN model. For the

MATLAB model the cross-section data comes from the ENDF-VIII cross-sections appended to the MCNP cross-section data. These two data sets have similar cross-section data for the thermal range but vary quite drastically in the epithermal and fast range. When comparing the measured data to the results of the two models it can be seen that the MATLAB model predicted between 40-50% less activity then measured and the ORIGEN model predicts anywhere from 30% less to 70% less depending on the isotope. The standard deviation of the difference between the measured and MATLAB predicted values, for all four isotopes, is only 6.18% whereas the standard deviation for ORIGEN is three times this value at 18.52%. Since all the MATLAB values are off by close to a constant factor it suggests that the ytterbium cross-sections from the ENDF-VIII library are more accurate than those from JEFF3.0/A. The average of the difference between the measured and MATLAB simulated activities is -45.82%. In order for the MATLAB results to match the measured activities the simulated power level of the reactor would have to be roughly 80% greater at 21.93 W instead of 12 W. This suggest that the actual operating power of the reactor was around 21.93 W instead of the measured 12 W. This is in agreement with the results obtain from the pool temperature analysis and gold foil calibration number derivation.

In addition to the activity of the four main product isotopes the percent activity of the sample that is due to Lu-177, the number of Lu-175 and Lu-177 atoms produced, and the specific activity of the lutetium was calculated with the MATLAB script and can be seen in Figure 4.12. The percent of the overall activity that is due to Lu-177 quickly reaches a value of around 1.2% after approximately 10 hours and then slowly increases over the next 40 hours to approximately 1.35%. The amount of Lu-177 produced can be seen in the bottom right corner of Figure 4.12 and shows that Lu-177 reaches its; peak amount after around 5-10 hours due to the short 1.9-hour half-life of the intermediate isotope, Yb-177, that it decays from. The amount of Lu-175 is still steadily increasing at the end of the 52-hour simulation due to the much longer 4.2-day half-life of its intermediate isotope, Yb-175. This large production of Lu-175 is the reason that the specific activity of the lutetium is so low and why it reaches its peak at the end of irradiation and only decreases from there. The maximum specific activity is seen to be approximately 55 Ci/mg and decreases all the way down to below 10 Ci/mg after 52 hours due to the continued growth of Lu-175 in the sample. It is for this reason that in order to obtain very high specific activity Lu-177, close to its theoretical CF specific activity of 111 Ci/mg, that ytterbium targets highly enriched in Yb-176 with the lowest content of Yb-174 are used.

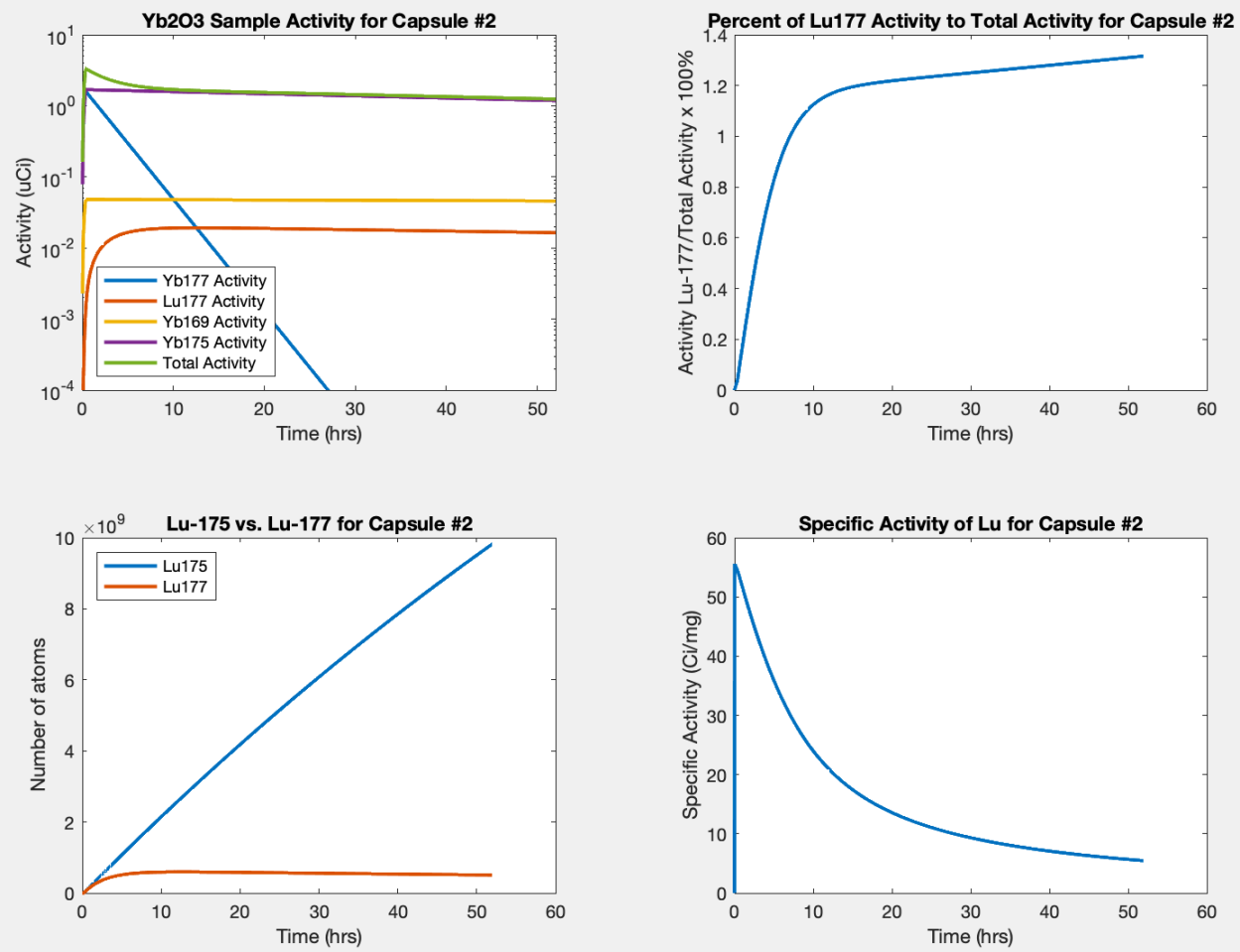


Figure 4.12. Sample activity, specific activity, Lu-175 and Lu-177 concentrations and percent Lu-177 activity to total sample activity.

## 4.4 High Power Irradiation

### 4.4.1 Detector Efficiency

The second sample to be irradiated was capsule #4 containing 9.362 grams of $Yb_2O_3$. This sample was actually irradiated twice, once for approximately 15 minutes at 9.0 kW and again the following day for approximately 4 hours and 10 minutes at 8.5 kW in the G6 irradiation assembly. Due to technical difficulties with the HPGe detector, located in the reactor laboratory, the sample did not have a sufficiently long gamma spectrum taken of it until it was shipped to and reached Niowave 11 days after the end of burnup (EOB). Despite this significant delay all of the four isotopes of interest, except for Yb-177 with its 1.9-hour half-life, were detectable in the

approximately one-hour gamma spectrum that was taken. The counts recorded for each peak were corrected to the true activities in the same way as sample #2 with two notable exceptions. In order to account for the efficiency of the detector a 2 mL liquid europium-152 calibration source was used to produce the efficiency curve of the detector as a function of energy, seen in Figure 4.13.

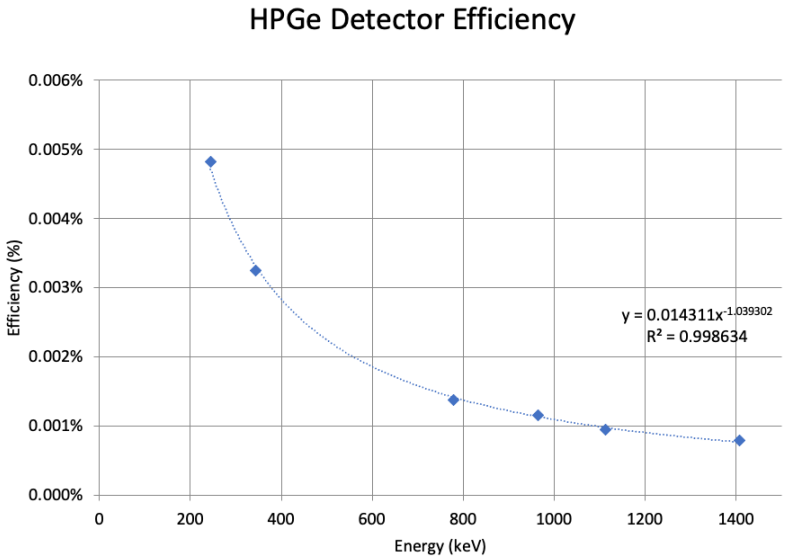


Figure 4.13. Niowave HPGe detector efficiency curve from Eu-152 source.

### 4.4.2 Gamma Attenuation Modeling

The second difference, in the method used to convert from counts to current activity, is the way that the gamma attenuation through the various materials to the detector was accounted for. For the first sample the attenuation was simplified as being for a point source through a constant thickness of each material. In reality the source is a finite cylindrical source, and the gamma attenuation is much more complicated. To more accurately account for gamma attenuation Niowave produced two simple MCNP models, one of the geometry of the ytterbium oxide sample in relation to the HPGe detector and one of the Eu-152 check source in relation to the detector. Then each MCNP model was run with several gamma tallies recorded for the cell containing the modeled detector with energy bins corresponding to the gamma energies of the four isotopes of interest. The ratio of the tallies, for each energy gamma, for the modeled ytterbium sample versus the modeled Eu-152 source was then determined. These ratios were then used as the attenuation factor for each gamma peak of interest. The results of these MCNP tallies can be seen in Table 4.4

and Figure 4.14. The method for converting measured counts to current activity is the same as for sample #2 except for that the detector efficiency is the one determined using the Eu-152 source at the Niowave facility, the gamma attenuation factor is replaced with the correction factor determined from the two MCNP trials and there is no counting time correction since the measurement was less than an hour and all the radioisotopes being measured have half -lives on the order of days.

Table 4.4. Gamma attenuation correction factor results provided thanks to Chad Denbrock and Jeremy Pike from Niowave Inc.

| **9.362 g Yb2O3 Attenuation Correction** | | | | | | | | | | |
|---|---|---|---|---|---|---|---|---|---|---|
| **Energy (keV)** | 109.8 | 113.4 | 150.4 | 177.2 | 198 | 208.4 | 282.5 | 396.3 | 1080.2 | 1241.8 |
| **Eu-152 Tally (x $10^{-7}$)** | 4.85 | 4.70 | 4.85 | 4.94 | 4.95 | 5.01 | 5.22 | 5.29 | 6.18 | 6.15 |
| **Yb2O3 Tally (x $10^{-7}$)** | 1.16 | 1.19 | 2.21 | 2.81 | 3.16 | 3.34 | 4.09 | 4.70 | 5.92 | 5.93 |
| **Correction (Yb/Eu)** | 0.240 | 0.254 | 0.456 | 0.570 | 0.639 | 0.666 | 0.784 | 0.889 | 0.958 | 0.964 |

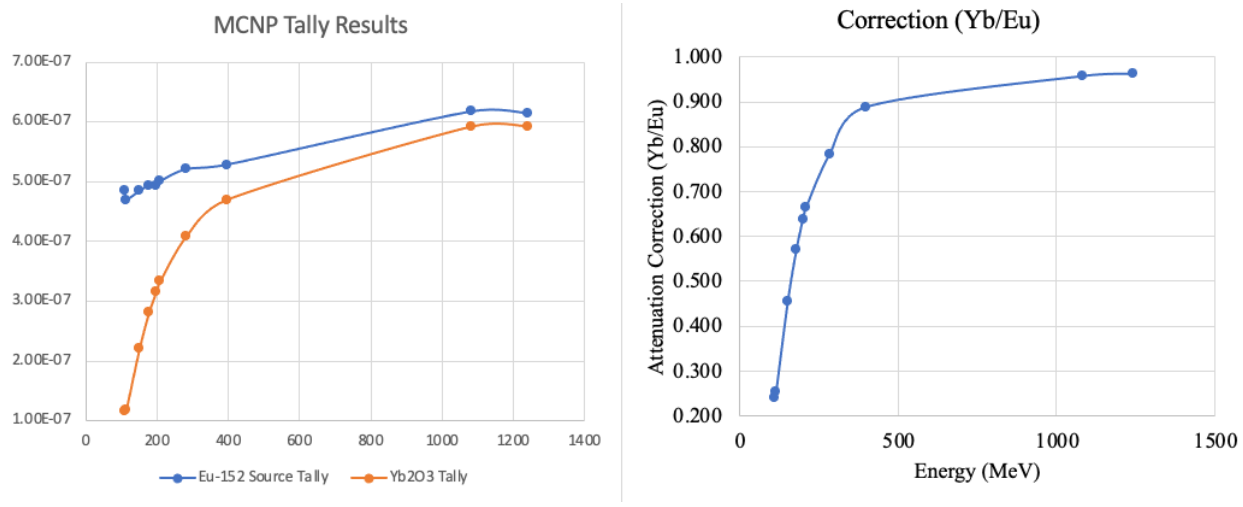


Figure 4.14. MCNP gamma tally results for gamma attenuation correction factor. Results provided thanks to Chad Denbrock and Jeremy Pike from Niowave Inc.

### 4.4.3 MATLAB and ORIGEN Modeling

With the current activities of the sample calculated both the MATLAB and ORIGEN model were used to simulate the irradiation and subsequent decay of sample #4. The ORIGEN model utilizes the 256-group neutron spectrum determined from the F4 tally of the cell containing the

9.362g of $Yb_2O_3$. The MATLAB model utilizes the reaction rates determined from the F4 tallies specified in the input for the 9.362g sample MCNP simulation. Information on the irradiation, both power level and duration, is available from the digital power data of PUR-1. This data shows that the average power of the first irradiation was 9.09 kW for a burnup of 2.4264 kW-hrs. This first burnup period is simulated with a step function power of 9.099 kW for 16 minutes. The second irradiation was at an average power of 8.505 kW for a burnup of 36.273 kW-hrs. This is simulated using with a step function power of 8.5015 kW for 4 hours and 16 minutes. The measured and simulated power levels for sample #4 can be seen in Figure 4.15.

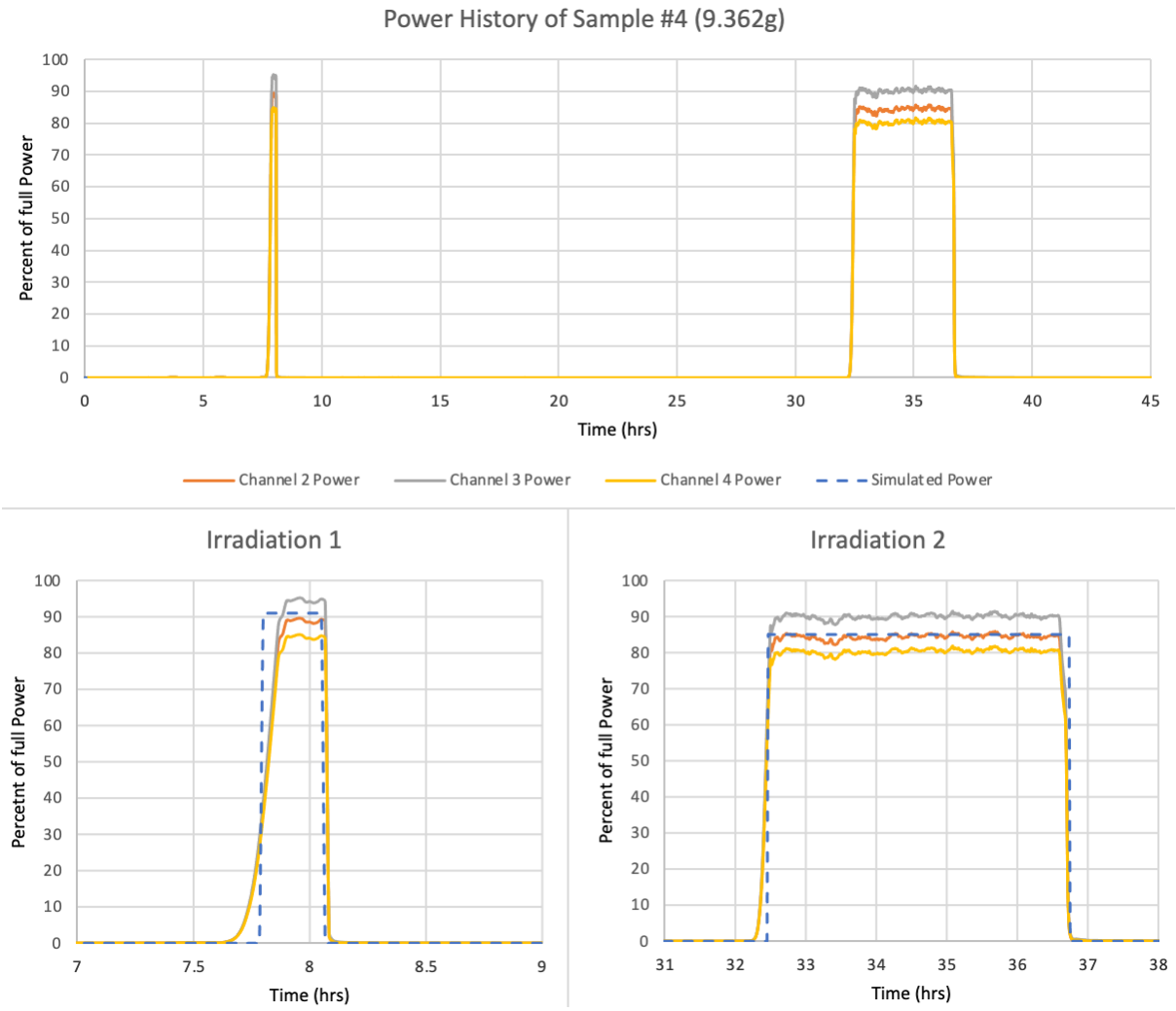


Figure 4.15. Power history for sample #4 and simulated power history.

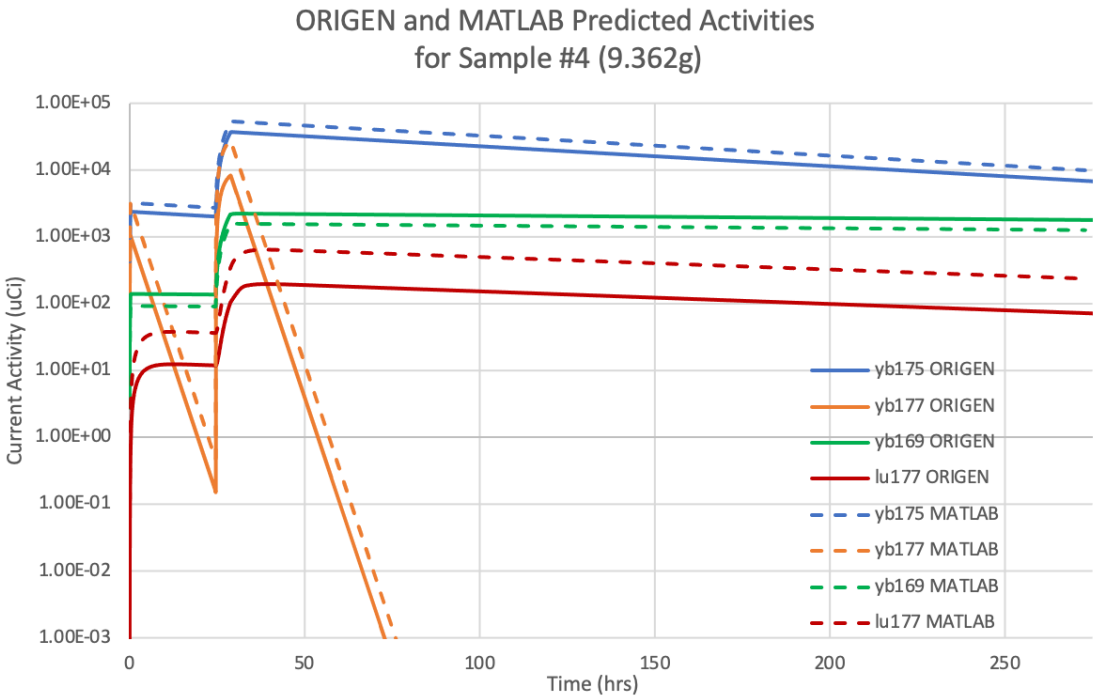


Figure 4.16. ORIGEN and MATLAB predicted isotope activities for sample #4.

Table 4.5. Measured and simulated isotope activities for sample #4.

| Isotope | Niowave (measured) Activity ($\mu$Ci) | MATLAB Activity ($\mu$Ci) | MATLAB % Difference | ORIGEN Activity ($\mu$Ci) | ORIGEN% Difference |
|---|---|---|---|---|---|
| **Yb-169** | 2036.95 | 1251.76 | -38.55% | 1775.62 | -12.83% |
| **Lu-177** | 355.40 | 226.46 | -36.28% | 68.62 | -80.69% |
| **Yb-175** | 14203.10 | 9205.84 | -35.18% | 6350.33 | -55.29% |

In Figure 4.16 and Table 4.5 the results of the MATLAB and ORIGEN simulations can be seen. Both models predicted similar behaviors the only differences between the two models are due to the different cross-section data used. Compared to the ENDF-VIII data the JEFF3.0/A cross-sections have a higher cross-section for Yb-169 and lower cross-sections for Yb-175, Yb-177 and Lu-177. This can be seen in the plot as the production of Yb-169 is overpredicted and the production of Yb-175, Yb-177 and Lu-177 is underpredicted compared to the MATLAB model. This difference can also be seen in the tabulated results of the measured activities and simulated activities of the two models in table 4.5. The MATLAB predicted activities for the three measured

isotopes are all less than the measured value by 35-38%. The average of these three percent differences is 36.67 percent less than the measured values and has a standard deviation of only 1.7%. This suggests that the cross-sections derived from the ENDF-VIII library are accurate for ytterbium and that the reason the simulated values are all off by a near constant value is because the measured power level, which was the value used in the simulations, was actually greater than what was reported. In order for the MATLAB simulation to match the measured results the core power would have to be approximately 14.2 kW instead of 9 kW, a roughly 60% increase in power.

In addition to the activities of each isotope of interest the MATLAB model also calculates the concentration of Lu-175 and Lu-177, the percent of total activity that is due to Lu-177 and the specific activity of the lutetium over time. As can be seen in Figure 4.17 the total amount of Lu-175 produced eclipses the amount of Lu-177. This is again because targets enriched in Yb-176 were not used and instead natural lutetium containing a large percentage of Yb-174 was used. The effect of this can be seen in the specific activity of the product material. It can be seen that the specific activity starts off high at 55 Ci/mg, around half the theoretical limit, but then quickly decreases after the irradiation stops and the Lu-175 starts to accumulate. When the second irradiation starts the specific activity can be seen to again rapidly increase this time only reaching around 35 Ci/mg and again quickly decreasing once the irradiation stops down to single digit values after several days. Despite the continued decrease in specific activity after the EOB the ratio of Lu-177 activity to total activity can be seen to steadily increase from around 1.25% to approximately 2.25% over the course of several days.

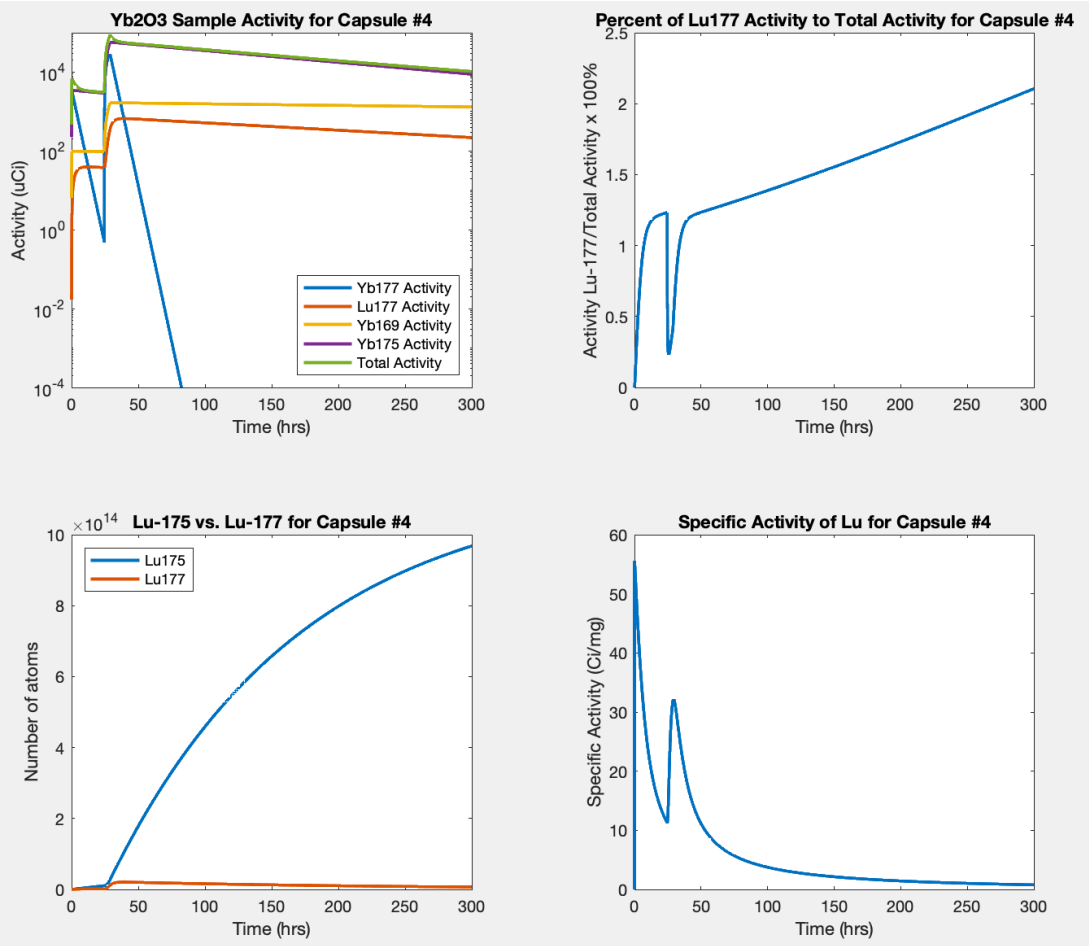


Figure 4.17. Sample activity, specific activity, Lu-175 and Lu-177 concentrations and percent Lu-177 activity to total sample activity.

## 4.5 Corrected Power Comparison

During the series of calibrations and experiments that make up this study, all the measured data and simulated results suggest that the core power was off by a factor of 60 to 80% of what was believed to be the measured value at that time. As a result, in order to compare each trial to the next, the average suggested power was found and reapplied to both the simulations and measured data in order to determine the level of agreement between each. To do this the average power that provides the best fit for each experiment or measurement was found and then the average of these five values taken. The resulting average core power deviation is 172.1% of the recorded values. Applying this correction to each calculation and experiment performed, results in an error of between +/-10% for almost all values except for the calculated Yb-177 activity for sample #2, which is off by just under -20%, and for the calculated activity of Yb-175 for sample

#4 which is off by just less than 12%. However, if the average of all differences for each sample is taken then the sample #2 average difference is -5.798% and the sample #4 average difference is 9.021%. This shows that all five measurements used to determine the true core power agree within +/-10%.

Table 4.6. Measured values vs. values calculated for 172.1% of recorded core power.

| | | Measured | Calculated | % Difference | Units |
|---|---|---|---|---|---|
| **Pool Temperature Change Rate** | | 0.54979 | 0.5209 | -5.25% | °C/hr |
| **Pool CFD Model** | | 15.0 | 14.63 | -2.47% | kW |
| **Gold Foil Calibration Constant** | | 2.93 | 3.115 | 6.31% | $\mu$Ci/100W-g-min |
| **Sample #2 Irradiation** | Lu-177 | 0.02943 | 0.0283 | -3.72% | $\mu$Ci |
| | Yb-177 | 0.91442 | 0.7373 | -19.37% | $\mu$Ci |
| | Yb-175 | 2.19241 | 2.0485 | -6.57% | $\mu$Ci |
| | Yb-169 | 0.07436 | 0.0792 | 6.47% | $\mu$Ci |
| **Sample #4 Irradiation** | Lu-177 | 355.4 | 389.8 | 9.69% | $\mu$Ci |
| | Yb-175 | 14203.1 | 15847.3 | 11.58% | $\mu$Ci |
| | Yb-169 | 2036.95 | 2154.8 | 5.79% | $\mu$Ci |

**Experiment Reactivity Worth**

The change in reactivity from the original core configuration for each experiment was an important value to be able to simulate in order to ensure that the reactivity worth insertion limit of plus or minus 400 pcm was not going to be exceeded. Simulations for each change in the core configuration were performed with the high-fidelity MCNP model. Each simulation was performed with 1E6 particles per cycle for 100 active cycles, this resulted in uncertainties all under 10 pcm. The first simulation was for the core with the control rods at a known critical rod height (CRH) and is used as the base model to compare the change in reactivity to. Five other simulations were then run; one with the graphite removed from the G6 irradiation tube, one with 4 empty capsules in the G6 irradiation port and then one each for each loading of ytterbium oxide loaded into the core, 0.258g, 2.455g and 9.362g.

The difference in reactivity of these simulations can be compared to the measured difference in reactivity calculated from the observed negative change rate of the reactor. The negative change rate, due to the change in core loading, was found by first finding the critical rod heights for the original, unchanged, core configuration. The graphite slug was then removed and the three dummy capsules and fourth capsule containing the ytterbium oxide was then loaded. This new core configuration was then brought to a critical state by keeping the SS1 and SS2 rods at the same critical location as the original core loading, and then by slowly removing the RR rod until a stable power was reached. Once the power was level, indicating a critical state, the RR rod was then inserted back to the critical height of the original core loading. The change rate is then able to be related to the reactivity worth through the use of the inhour equation seen below.

$$\rho = \frac{\Lambda}{T_p} + \sum_{i=1}^{6} \frac{\beta_i}{1+\lambda_i T_p} \qquad\qquad T_P = \frac{1}{C.R.}$$

Where $\rho$ is reactivity in %k/k, $\Lambda$ is the mean neutron generation time, $T_p$ is the reactor period and $\beta_i$ and $\lambda_i$ are the 6 group delayed neutron fractions and precursor decay constants. The reactor period can be calculated from the power change rate using the equation seen above. The values for the mean neutron generation time and 6 group delayed neutron fractions and precursor decay constants were found using the KOPTS output card option in MCNP which outputs the point kinetics parameters of the model seen below [10].

Table 4.7. Point kinetics parameters of PUR-1.

| $\boldsymbol{\beta_i}$ | (%) | $\boldsymbol{\lambda_i}$ | (s^-1) |
|---|---|---|---|
| $\boldsymbol{\beta_1}$ | 0.00028 | $\lambda_1$ | 0.01334 |
| $\boldsymbol{\beta_2}$ | 0.00122 | $\lambda_2$ | 0.03273 |
| $\boldsymbol{\beta_3}$ | 0.00161 | $\lambda_3$ | 0.1208 |
| $\boldsymbol{\beta_4}$ | 0.0033 | $\lambda_4$ | 0.30294 |
| $\boldsymbol{\beta_5}$ | 0.00138 | $\lambda_5$ | 0.85024 |
| $\boldsymbol{\beta_6}$ | 0.00056 | $\lambda_6$ | 2.85582 |
| $\boldsymbol{\Lambda}$ | 7.36E-05 | s | |

The first MCNP test case of the CRH configuration resulted in a $k_{eff}$ 21 pcm below critical. The remaining cases were compared to this case and their difference in $k_{eff}$ used to calculate the reactivity difference from this base case. The removal of the graphite rod was responsible for -88 pcm of reactivity due to a decrease in moderation and reflection. The addition of the 4 empty aluminum capsules into where the graphite rod once was actually resulted in an increase of 10 pcm of reactivity over just having air in the irradiation tube. This is due to the increase in reflection. The three simulations, with varying amounts of ytterbium oxide in the fourth capsule, showed a small increase in negative reactivity with the increase of the mass of $Yb_2O_3$. The MCNP predicted reactivity differences for the 0.258g, 2.455g, and 9.362g samples were -81, -92 and -99 pcm respectively, well below the limit of 400 pcm. The calculated reactivities for these three cases, based on the measured change rates, resulted in negative reactivity worths significantly less than predicted by MCNP. The calculated reactivity worths of the 0.258g, 2.455g, and 9.362g samples were -47.5, -49.3 and -53.2 pcm respectively. Although the MCNP model predicts values just under double the calculated values they are still well within the same order of magnitude and it is better for the model to overpredict then underpredict the reactivity worth of the core changes to error on the side of caution.

Table 4.8. Calculated and simulated reactivity worths of various core loadings.

| Case | $k_{eff}$ | +/- | Difference (pcm) | Crit. RR height (cm) | Change rate (%/s) | $T_P$ (s) | rho (pcm) | Difference (%) |
|---|---|---|---|---|---|---|---|---|
| **CRH** | 0.99979 | 0.00007 | 0 | 29.96 | - | - | - | - |
| **Graphite Removed** | 0.99891 | 0.00006 | -88 | - | - | - | - | - |
| **4 empty capsules (0g)** | 0.99901 | 0.00007 | -78 | - | - | - | - | - |
| **0.258g** | 0.99898 | 0.00008 | -81 | 37.32 | -0.4639 | 216.05 | -47.5 | -41.4% |
| **2.455g** | 0.99887 | 0.00009 | -92 | 37.65 | -0.4780 | 209.72 | -49.3 | -46.4% |
| **9.362g** | 0.9988 | 0.00008 | -99 | 38.32 | -0.5071 | 197.70 | -53.2 | -46.3% |

In Figure 4.18 the recorded power level and reactor power change rate for sample #1 can be seen. The left circled region of the plot shows the power change rate when the power is level

indicating a critical state. The second circled region shows the power change rate for after the RR rod was inserted to its previously critical position for when no changes had been made. The difference between the average of each of these regions was then taken and used to determine the reactor period and with the reactor period known the inhour equation was then used to determine the reactivity worth of the core loading.

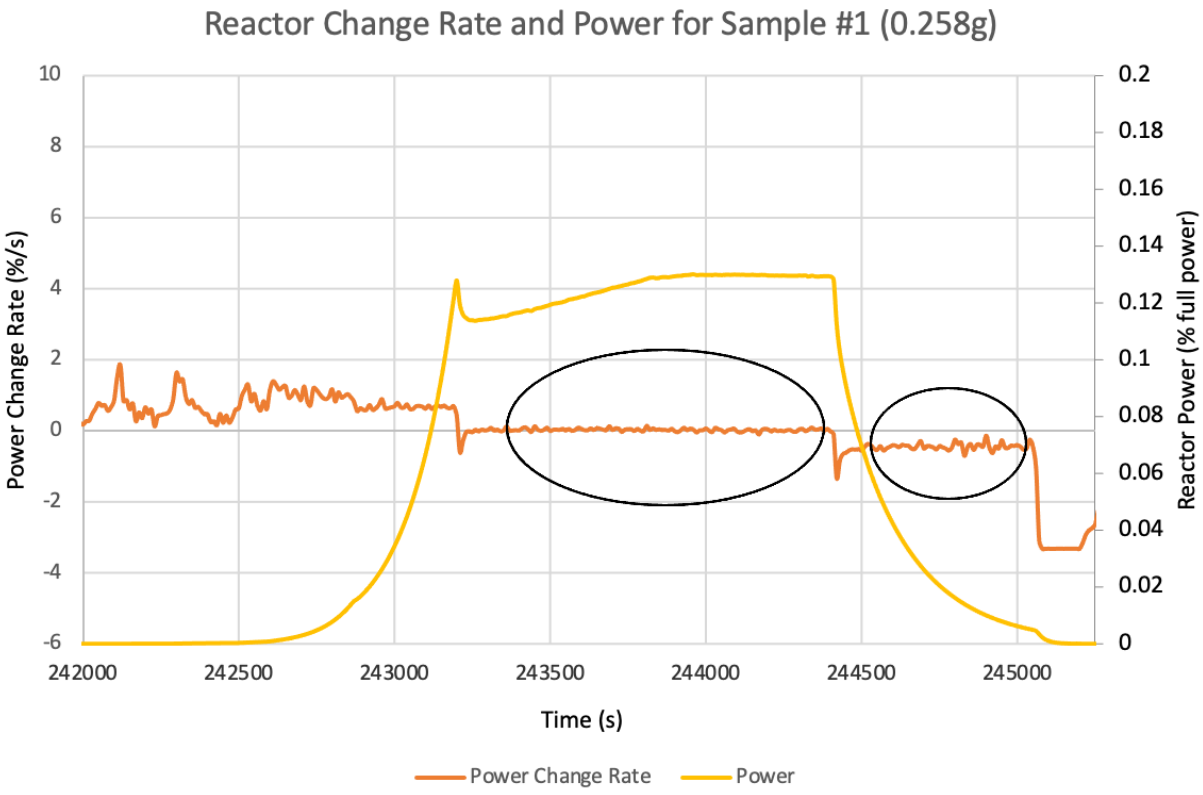


Figure 4.18. Reactor power versus power change rate for sample #1.

# 5. FUTURE WORK AND IMPROVEMENTS

## 5.1 Core Reconfiguration

There are two possible ways to increase the production rate of Lu-177, either utilize targets enriched in Yb-176 or increase the flux that the target is exposed to. One possible way to increase the flux the target material receives without increasing the operating power of the core is to reconfigure the assemblies to have an irradiation assembly in an interior location of the core, surrounded by fuel elements. Two different interior locations were tested for this core arrangement. One involving swapping the irradiation assembly currently at G6 with the fuel element located at G4. The other configuration is similar this time swapping the F6 irradiation assembly with the F4 fuel assembly. In order to provide increased moderation and reflection for the fuel element now in row 6, two reflector assemblies from the opposite corners of the core and a third extra reflector assembly would be placed around the relocated fuel assembly. With no other changes to the core these configurations are subcritical even with ARO. If 16 more fuel plates are added to the core in place of the dummy plates, bring the total to 206 fuel plates. The row G swapped configuration will have 72 pcm of excess reactivity with ARO and the row F swap configuration will have 167 pcm of excess reactivity with ARO. The total flux, at 10 kW, predicted for these configurations would be approximately 6.6E11 and 6.3E11 and the thermal flux would be approximately 2.6E11 and 2.3E11. This new configuration would result in a 61.4% increase in reaction rates for the row G swap configuration and a 48.8% increase for the row F swap configuration based on F4 (n, $\gamma$) tallies from the MCNP outputs. Both simulated core reconfigurations can be seen in Figure 5.1.

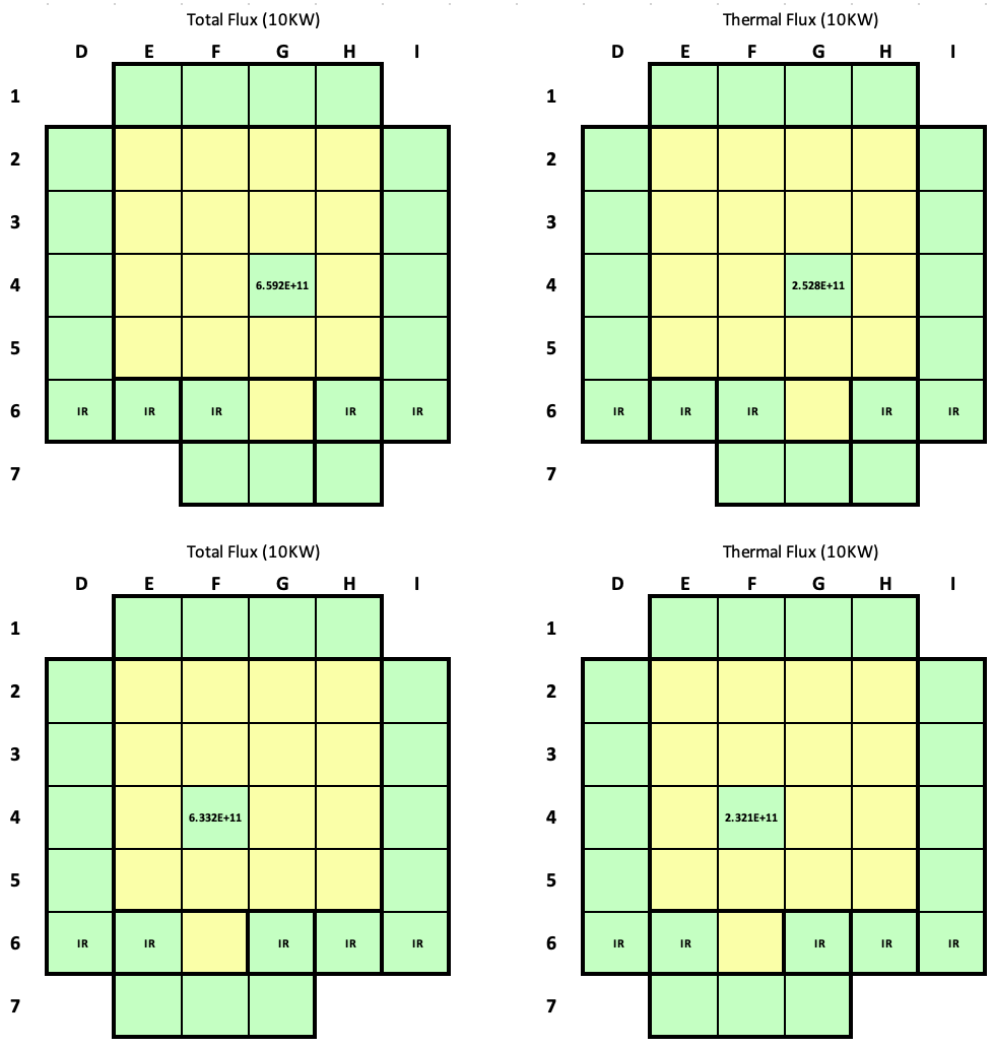


Figure 5.1. Possible alternative core configurations for increased production.

## 5.2 Target Enrichment

The second method to increase the production rate of Lu-177 would be to use an enriched target and to perform multiple irradiations over an extended period of time. To model this a MCNP simulation was ran with the maximum amount of ytterbium oxide that will fit in the HDPE vial in the capsule. This amount is equal to 28.6 grams when the material is compressed to 5.5 g/cc. The material composition of the ytterbium oxide in the MCNP model was then changed to be 97% Yb-176, which is the highest enrichment level I could find commercially available. The concentration of the remaining isotopes of Yb are not listed so it is assumed that the remaining 3% is composed of equal parts Yb-174, Yb-173 and Yb-172. F4 tallies were then performed on this new material to determine reaction rates that were then used as inputs for the MATLAB model. In the MATLAB

model the power is set to 10 kW and five 6-hour irradiation are model with 18-hour cooldown periods between each. The resulting activities of each isotope, the concentration of Lu-177 and Lu-175, specific activity of the produced lutetium and the percent of the total activity that is due to Lu-177 can be seen in Figures 5.2 and 5.3 below.

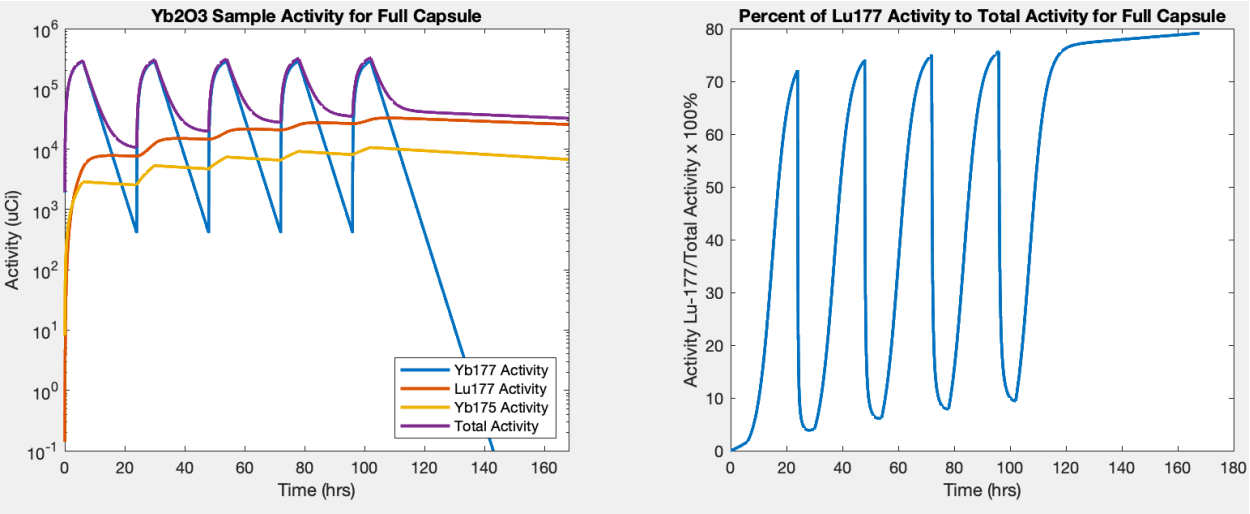


Figure 5.2. Activity of each product isotope and percent of the total activity due to Lu-177.

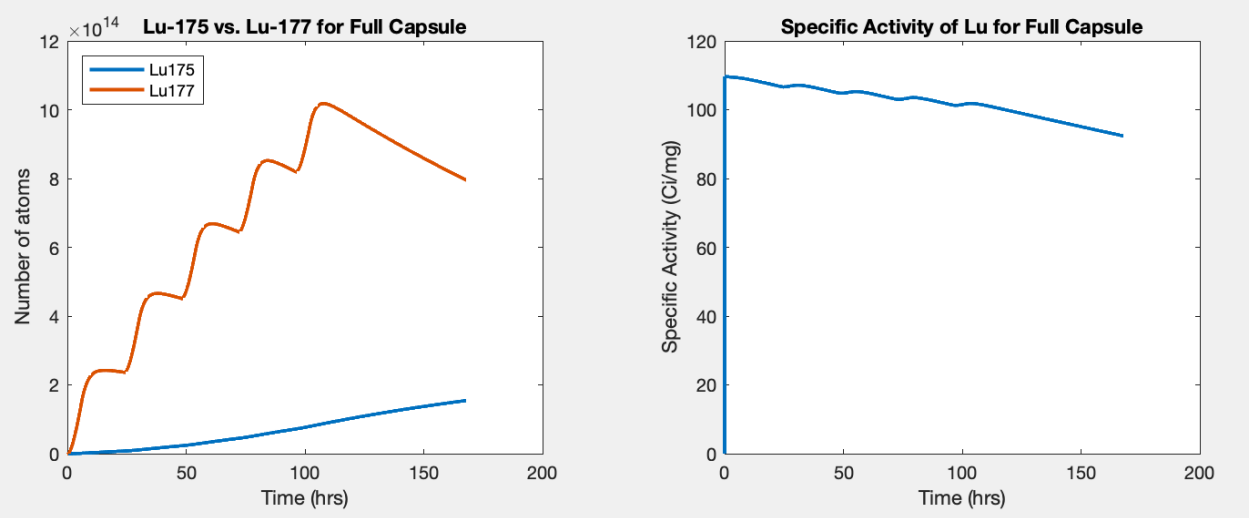


Figure 5.3. Concentration of Lu-177 and Lu-155 and the specific activity of the lutetium produced.

It can be seen in Figure 5.2 that while Yb-177 is being actively produced during irradiation, that this isotope is responsible for the majority of the activity of the target material. However, since

this isotope has such a short half-life after the reactor is powered down the majority of the radiation will be due to Lu-177. During irradiation roughly 10 to 15% of the activity of the sample is Lu-177 but this value quickly shifts to being 70 to 75% of the total activity during the cooldown periods and slowly grows to represent 80% of the total activity after one week. Loading a capsule with the maximum amount of enriched ytterbium oxide also results in a very large amount of Lu-177 being produced after the fifth irradiation. After the end of the five irradiations the amount of Yb-177 slowly increases to its peak activity of 32.94 mCi, which it reaches six hours after the end of the last irradiation. After two more days the activity is still very considerable at 25.73 mCi. Not only is the amount of Lu-177 greatly increased but the ratio of Lu-177 to Lu-175 produced is much greater compared to using natural ytterbium, this results in a very high quality NCA grade specific activity of Lu-177. At the end of the fifth irradiation the specific activity is 101.74 Ci/mg which is 92.4% of the theoretical CF specific activity of Lu-177. This value only drops to 92.35 Ci/mg two days after the end of the last irradiation, which is still 84% of the CF specific activity. Utilizing a fully loaded capsule of enriched ytterbium oxide with multiple days of irradiation would result in a considerable quantity of NCA quality Lu-177.

# 6. CONCLUSIONS

The production of NCA specific activity lutetium-177 is becoming more and more important for a number of different TRT applications. Due to the high thermal flux requirements the direct route of production is not achievable for many countries that lack powerful research reactors. Additionally, due to the inability to separate the produced Lu-177 from the remainder of the target material, the direct route is not capable of producing the high specific activities required for certain applications such as Lu-177 labeled immunotherapy. The indirect route is able to be achieved in research reactors of almost all powers and has the greatest potential for near CF specific activities when using Yb-176 enriched target materials. Despite not using enriched ytterbium oxide this study shows that with enriched targets it is feasible to produce a sizeable quantity of Lu-177 of NCA specific activity using PUR-1.

A high fidelity MCNP model of PUR-1 was developed for this project and showed great accuracy in reproducing measured excess reactivity, control rod worths, critical rod heights and flux distributions. This MCNP model in conjunction with both the ORIGEN burnup model and the simplified MATLAB script were able to accurately predict the production and decay of all the product isotopes of interest with minimal error. The MATLAB model, whose inputs are based on the ENDF-VIII cross-sections show better agreement with the measured data then the results of the ORIGEN model which uses JEFF3.0/A cross-section data. For future models ENDF-VIII cross-section data will be used. The combination of a Monte Carlo based model to determine reaction rates with a simplified finite difference system, for solving the system of partial differential equations describing the production and decay of each product isotope, proved to be a powerful tool for predicting the results for any target loading irradiation power and duration. This method is applicable for the modeling of any type of isotope production that uses a research reactor as the neutron source.

The irradiation of two samples of ytterbium oxide were successfully performed during the course of this experiment. One 2.455g sample was irradiated for a short period of time at lower power and one 9.362g sample was irradiated twice at high power and for a much longer duration. The resulting activities of each product isotope produced were successfully determined from the gamma spectrums recorded from the irradiated samples. The first sample's gamma attenuation factor was approximated by a point source with constant thickness materials. This simplification

may have resulted in a certain degree of error for the final calculated activities. The resulting simulated activities of each product isotope were off by an average difference of -45.82 % of the calculated activities with a standard deviation of 6.18%. This simplified method of determining the gamma attenuation may have resulted in a 5 to 10% error in the calculated isotope activities but all four isotopes being off by an average of 40 to 50% suggests that the true operating power of the core was approximately 80% greater than thought. The second successful irradiation resulted in similar results to the first irradiation. The resulting simulated activities of each product isotope were off by an average difference of -36.67 % of the calculated activities with a standard deviation of only 1.70%. The results of this second irradiation suggest that using the difference in gamma tallies between two separate MCNP models, both modeling the source and detector geometry is a much more accurate method for accounting for gamma attenuation due to the very small standard deviation of the percent differences of each isotope. The average difference of all three isotopes also suggest that the true core power was approximately 60% greater than it was thought to be.

In addition to the two successful irradiation measurements, data of the pool water temperature during the high-power irradiation was recorded to determine the true reactor power and the gold foil calibration constant was derived using the MCNP model developed for this study. The measured rate of change of the coolant temperature throughout the 4-hour irradiation trial initial suggested that the reactor was operating at 15.4 kW which is roughly 80% greater than the 8.5 kW of power that we thought we were operating at. A CFD simulation of PUR-1 was performed by Dr. Ran Kong and these results also supported the conclusion that the true reactor power was between 14 to 15.5 kW. To determine if the power calibration constant is accurate the value was rederived using the results from several MCNP tallies. The resulting calculated value is 1.8095 $\mu$Ci/100W-g-min this is 38.2% less than the value currently used. Using the original value of 2.93 $\mu$Ci/100W-g-min would result in a power approximately 62% greater than expected. All five of these experiments and calculations show that the reactor power was between 60 - 80% greater than the measured power. When the measured value was adjusted by the average suggest power value of 172.144% all five experiments and measurements show agreement withing +/- 10% which strongly suggests the calibrated core power was off by a significant amount.

This experiment required multiple models and calibrations to be able to both simulate and predict as well as measure and calculate the concentrations and activities of the product isotopes produced from the irradiation of the natural ytterbium oxide targets. While NCA specific activity

Lu-177 was not produced in this experiment a suitable amount of Lu-177 of lower quality was produced allowing Niowave to test several chemical separation techniques before more expensive enriched target material is used. Additionally, after correcting for core power discrepancies, it was shown that the MCNP model in connection with the finite difference production and decay model is able to very accurate predict the isotopic composition for any given run. When these tools are used to simulate an enriched target material with a multiday burnup a significant amount of NCA grade Lu-177 is predicted to be produced. Due to the accuracy producing the results of the first two experiments it is safe to say that the production of NCA Lu-177, using PUR-1, is very feasible.

# REFERENCES


[1] Dash, A. (2017, April 07). Reactor-produced therapeutic radionuclides. Retrieved April 09, 2021, from https://radiologykey.com/reactor-produced-therapeutic-radionuclides/

[2] Samarium SM 153 Lexidronam (INTRAVENOUS Route) description and brand names. (2021, February 01). Retrieved April 09, 2021, from https://www.mayoclinic.org/drugs-supplements/samarium-sm-153-lexidronam-intravenous-route/description/drg-20065896

[3] Avuzzi, B., & Valdagni, R. (2016). Bone metastases from prostate cancer: Radiotherapy. *Bone Metastases from Prostate Cancer,* 163-180. doi:10.1007/978-3-319-42327-2_14

[4] Sodium iodide i 131 (Oral Route) description and brand names. (2021, February 01). Retrieved April 09, 2021, from https://www.mayoclinic.org/drugs-supplements/sodium-iodide-i-131-oral-route/description/drg-20066049

[5] Dash, A., Pillai, M. R., & Knapp, F. F. (2015). Production of 177Lu for Targeted Radionuclide Therapy: Available options. *Nuclear Medicine and Molecular Imaging, 49*(2), 85-107. doi:10.1007/s13139-014-0315-z

[6] Tikhonchev, M. Y., Svetukhin, V. V., Novikov, S. G., Bil'danov, R. G., & Il'in, K. I. (2019). 177Lu accumulation parameters in different nuclear reactors. *Atomic Energy, 125*(6), 376-383. doi:10.1007/s10512-019-00497-2

[7] RSICC CODE PACKAGE CCC-850. (n.d.). Retrieved April 09, 2021, from https://rsicc.ornl.gov/codes/ccc/ccc8/ccc-850.html

[8] Bean, R. S., & Storz, D. L. (2015). *PUR-1 Operating Principles and Core Characteristics Manual* (Rep.). West Lafayette, IN: Purdue University.

[9] Neubert, T., Royal, J., & Van Dyken, A. (1956). The structure and properties of artificial and natural graphite. doi:10.2172/4360150

[10] Armstrong, J., Brown, et. al. (2017). *MCNP Users's Manual Code Version 6.2* (Tech.). Los Alamos, New Mexico: Los Alamos National Laboratory.

[11] Rearden, B. T., & Jessee, M. A. (2018). *Scale Code System Version 6.2.3* (Tech.). Oak Ridge, TN: Oak Ridge National Laboratory.

[12] Harms, G. A. (1981). Neutron Flux Characterization by Spectrum unfolding in PUR-1. *Purdue Doctoral Thesis*.